HHS Public Access
Author manuscript
*Cell Rep*. Author manuscript; available in PMC 2024 October 02.

Published in final edited form as:
*Cell Rep*. 2024 July 23; 43(7): 114380. doi:10.1016/j.celrep.2024.114380.

# Cell-specific regulation of the circadian clock by BMAL1 in the paraventricular nucleus: Implications for regulation of systemic biological rhythms

**Rachel Van Drunen**[1,2], **Yulin Dai**[3], **Haichao Wei**[1,4], **Baharan Fekry**[1], **Sina Noori**[1], **Samay Shivshankar**[1], **Rafael Bravo**[1], **Zhongming Zhao**[3], **Seung-hee Yoo**[2,5], **Nicholas Justice**[1,2,6], **Jia Qian Wu**[1,2,4], **Qingchun Tong**[1,2], **Kristin Eckel-Mahan**[1,2,7,*]

[1]UT Brown Foundation Institute of Molecular Medicine, University of Texas Health Science Center at Houston, Houston, TX 77030, USA

[2]MD Anderson Cancer Center/UTHealth Graduate School of Biomedical Sciences, University of Texas Health Science Center at Houston, Houston, TX 77030, USA

[3]Center for Precision Health, McWilliams School of Biomedical Informatics, University of Texas Health Science Center at Houston, Houston, TX 77030, USA

[4]Department of Neurosurgery, University of Texas Health Science Center at Houston, Houston, TX 77030, USA

[5]Department of Biochemistry and Cell Biology, University of Texas Health Science Center at Houston, Houston, TX 77030, USA

[6]Department of Integrative Biology and Pharmacology, McGovern Medical School, University of Texas Health Science Center at Houston, Houston, TX 77030, USA

[7]Lead contact

## SUMMARY

Circadian rhythms are internal biological rhythms driving temporal tissue-specific, metabolic programs. Loss of the circadian transcription factor BMAL1 in the paraventricular nucleus (PVN) of the hypothalamus reveals its importance in metabolic rhythms, but its functions in individual PVN cells are poorly understood. Here, loss of BMAL1 in the PVN results in arrhythmicity of processes controlling energy balance and alters peripheral diurnal gene expression. BMAL1 chromatin immunoprecipitation sequencing (ChIP-seq) and single-nucleus

---

This is an open access article under the CC BY-NC-ND license (http://creativecommons.org/licenses/by-nc-nd/4.0/).

[*]Correspondence: kristin.l.mahan@uth.tmc.edu.

AUTHOR CONTRIBUTIONS

K.E.-M. and R.V.D. conceived the study with contributions from Q.T., J.Q.W., N.J., and S.-h.Y. R.V.D. performed experiments with contributions from B.F., S.N., S.S., and R.B. snRNA-seq analysis was carried out by Y.D. under the guidance of Z.Z. H.W. performed ChIP-seq analysis under guidance of J.W. Analysis of the snRNAseq and the ChIP-seq was carried out by R.V.D. and K.E.-M. R.V.D. and K.E.-M. wrote the manuscript with input from co-authors Q.T., J.Q.W., S.Y., and N.J. K.E.-M. supervised the study and was responsible for the funding.

SUPPLEMENTAL INFORMATION

Supplemental information can be found online at https://doi.org/10.1016/j.celrep.2024.114380.

DECLARATION OF INTERESTS

The authors declare no competing interests.

Author Manuscript Author Manuscript Author Manuscript Author Manuscript

Author Manuscript

Author Manuscript

Author Manuscript

Author Manuscript

RNA sequencing (snRNA-seq) reveal its temporal regulation of target genes, including oxytocin (OXT), and restoring circulating OXT peaks in BMAL1-PVN knockout (KO) mice rescues absent activity rhythms. While glutamatergic neurons undergo day/night changes in expression of genes involved in cell morphogenesis, astrocytes and oligodendrocytes show gene expression changes in cytoskeletal organization and oxidative phosphorylation. Collectively, our findings show diurnal gene regulation in neuronal and non-neuronal PVN cells and that BMAL1 contributes to diurnal OXT secretion, which is important for systemic diurnal rhythms.

## Graphical abstract

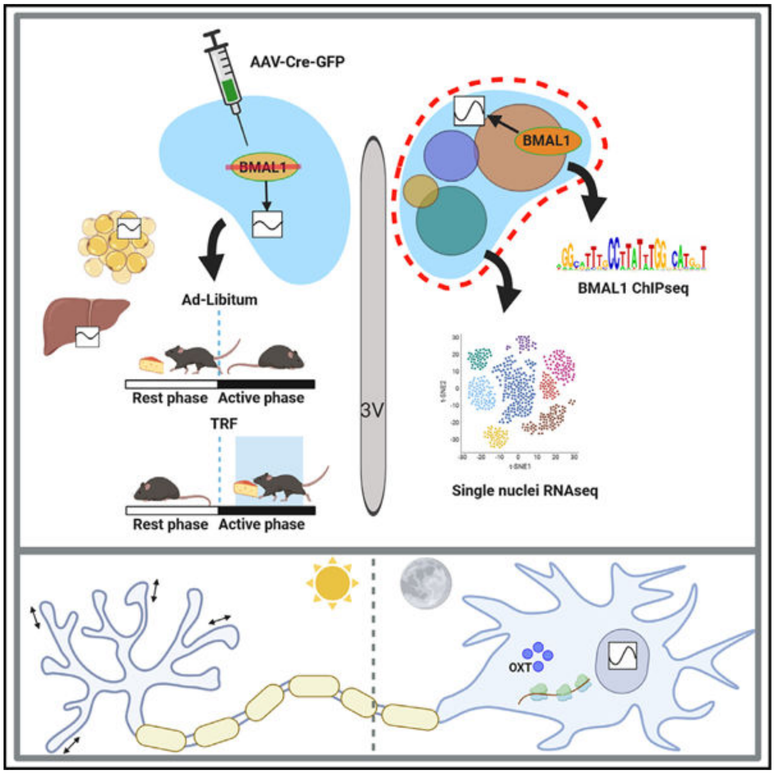

## In brief

Diurnal gene expression in the paraventricular nucleus (PVN) of the hypothalamus is highly dynamic and cell specific. Van Drunen et al. demonstrate mechanisms by which the circadian transcription factor BMAL1 drives PVN gene regulation and, subsequently, rhythmicity in energy intake and expenditure.

## INTRODUCTION

Energy balance is achieved by tight regulation of energy intake and energy expenditure, metabolic processes that undergo variations across the day/night cycle.[1–3] Metabolism, feeding, and other aspects of physiology, including the sleep/wake cycle are regulated internally by a 24-h intrinsic biological clock. While circadian rhythms can be found in nearly every cell and tissue of the body, mammalian clocks are synchronized by the

Author Manuscript Author Manuscript Author Manuscript Author Manuscript

suprachiasmatic nucleus (SCN) of the hypothalamus, which receives daily input from light-sensing, melanopsin-containing retinal ganglion cells.[4–6] Other environmental cues, or zeitgebers (meaning "time givers"), such as food intake, can also entrain the circadian clock in specific tissues.[7–11]

Though the SCN is considered the light-responsive circadian pacemaker of the brain,[12] the circadian clock is present throughout the brain, where it regulates complex functions such as olfaction,[13] learning and memory,[14] addiction,[15] and mood.[16] Studies have underscored the importance of the hypothalamic circadian clock in controlling energy balance.[17–21] Nutrient-related signals from other hypothalamic nuclei are relayed to the paraventricular nucleus (PVN), located in the mediobasal hypothalamus, which relays satiety signals to downstream brain regions to control metabolism, feeding, and hormone production.[22–26] The PVN clock also contributes to diurnal regulation of metabolic processes and glucocorticoid rhythms.[19,20,27]

The cellular mammalian clock is characterized by a negative transcriptional/translational feedback loop. Brain and muscle ARNTL-like 1 (BMAL1) and circadian locomotor output cycles kaput (CLOCK) heterodimerize and promote transcription of thousands of genes, including the period (PER) and cryptochrome (CRY) genes, which subsequently block transcriptional activation by CLOCK:BMAL1. In peripheral organs, where BMAL1 has been well characterized for its chromatin regulation, BMAL1 recruitment to chromatin is dynamic, peaking in the resting phase (zeitgeber time 6 [ZT6]–ZT10). Global loss of BMAL1 results in arrhythmicity and accelerated aging,[28] while tissue-specific loss of BMAL1 results in tissue-specific metabolic defects.[29–31] Forebrain and SCN-specific loss results in arrhythmicity in free-running conditions,[32] while nestin-driven BMAL1 deletion causes temporary entrainment deficiencies under periodic feeding that are eventually overcome.[33] Constitutive synaptotagmin 10 (*Syt10*) promoter-driven BMAL1 loss in the SCN also results in arrhythmicity in free-running conditions but not in entrained conditions.[34] Astrocyte-specific deletion of BMAL1 results in impaired GABA uptake at synapses, early onset astrogliosis, and changes in circadian periodicity.[35–38] Interestingly, loss of BMAL1 only in corticotrophin-releasing neurons of the PVN dampens daily corticosterone release.[20]

Remarkably, loss of BMAL1 in the PVN causes obesity and reduces diurnal rhythmicity in metabolism, even in entrained conditions.[19] To understand mechanisms by which the circadian clock in the PVN regulates rhythmic physiology and metabolism, we used adeno-associated Cre (AAV-CRE)-expressing virus to drive PVN-specific loss of BMAL1 in Bmal1$^{flox/flox}$ mice of both sexes. In addition to disrupted 24-h activity, mice with PVN BMAL1 deficiency show peripheral tissue rhythm defects. Using chromatin immunoprecipitation sequencing (ChIP-seq), we reveal widespread genomic occupancy by BMAL1 in the PVN at loci important for synaptic plasticity and neuronal function. To characterize cell-type-specific and diurnal transcriptional changes in the PVN, we also carried out single-cell nucleus RNA sequencing (snRNA-seq) at two antiphase time points. Classification of PVN cell types revealed profound circadian-dependent changes in gene expression. Specifically, we find pronounced diurnal changes in expression of synaptic organization and plasticity-related genes in astrocytes, oligodendrocytes, and glutamatergic

Author Manuscript

Author Manuscript

Author Manuscript

Author Manuscript

and GABAergic neurons. In addition, we observed highly diurnal expression of the neuropeptide oxytocin (OXT), which was altered in the absence of BMAL1. Interestingly, restoring peak circulating OXT in PVN BMAL1-deficient mice counteracts their arrhythmic behavior. Taken together, our findings provide a strong basis for BMAL1-driven regulation of the PVN clock, which contributes to daily, organism-wide rhythmicity.

## RESULTS

### BMAL1 deletion in the PVN disrupts energy balance and diurnal rhythms of activity

To study the role of the PVN clock in rhythmicity, we deleted BMAL1 in the PVN of *Bmal1*$^{\mathrm{fl/fl}}$ mice by stereotaxic delivery of AAV-expressing GFP (control) or Cre-GFP (BMAL1-PVN knockout [KO]) into the PVN (Figures 1A and S1A). Male and female BMAL1-PVN KO mice displayed increased body weight (Figures 1B and S1B) and loss of 24-h activity rhythms compared to controls (Figures 1C and S1C–S1H), with rhythmicity prior to Cre-GFP injection being normal (Figures S1C and S1F–S1H). For a small number of BMAL1-PVN KO mice, a 24-h period could still be determined (Figure 1D, "*ad libitum*"), though activity rhythms were greatly reduced (Figures S1G and S1H). Because BMAL1-PVN KO mice lost rhythmicity in entrained conditions, we tested whether the SCN maintained light responsiveness. BMAL1-PVN KO mice were placed in free running, constant dark conditions for 10 days, and provided either no light, or a 30-min 6.2 lumen/ft$^2$ light pulse administered at circadian time 19 (CT19). SCNs were harvested, and expression of the immediate-early gene c-Fos was analyzed. Compared to no light pulse, light potently activated c-Fos in the SCN, suggesting that BMAL1-PVN KO mice did not suffer from defective SCN light sensing (Figures 1E and 1F). However, the SCN BMAL1 target genes *Reverbβ* and *Per2* showed antiphase expression compared to that expected in nocturnal mice (Figures 1G and 1H).

Based on the disrupted food intake in BMAL1-PVN KO mice,[19] we tested whether restoring diurnal energy intake would rescue activity rhythms. BMAL1-PVN KO mice were placed on 10-h (ZT13–ZT23) time-restricted feeding (TRF) for 2 weeks. By week 2 of TRF, BMAL1-PVN KO mice began to display diurnal rhythms (Figures 1C and 1D) and increased day/night changes in home cage activity (Figures 1I and 1J). Under *ad libitum* feeding, BMAL1-PVN KO mice displayed minimal changes in day vs. night activity, energy expenditure, and energy intake, emphasizing loss of entrainment (Figures S1I and S1J), and total energy intake was invariant compared to control mice (Figure S1K). However, under TRF, BMAL1-PVN KO mice showed significant increases in night vs. day activity (Figures 1K–1M), though daily food consumption was invariant from controls (Figure S1L). MRI revealed that TRF did not significantly change fat or lean mass when comparing groups (Figure S1M).

Notably, loss of BMAL1 in the PVN disrupted diurnal gene expression in the liver and inguinal and epididymal white adipose tissue (iWAT and eWAT, respectively) at ZT8 and ZT20. This was reflected by altered expression of *Bmal1* and the albumin D box binding protein *Dbp* as well as the lipid metabolism gene fatty acid synthase (*Fas*) (Figures 1O, 1P, and S1N; Data S1). TRF-induced changes were particularly robust for *Bmal1* in iWAT and for *Dbp* in the liver (Figures 1O, 1P, and S1N; Data S1). These findings suggest that

Author Manuscript

Author Manuscript

Author Manuscript

Author Manuscript

TRF can partially rescue BMAL1-deficient PVN-mediated defects in diurnal behavior and peripheral gene expression.

## BMAL1 binds to numerous genomic loci in the PVN in a diurnal pattern

Though BMAL1 genomic regulation in some peripheral tissues has been studied extensively,[39–43] less is known about BMAL1 targets across the CNS. We used ChIP-seq to identify BMAL1 targets in PVN-enriched tissue dissected at ZT8 (reflecting peak binding in the liver[39,40]) (Figure 2A). ChIP-seq revealed a total of 663 genomic regions bound by BMAL1, which include the known targets *Dbp* and *Per2* (Figure S2A). Binding within 3 kb of the transcriptional start site (TSS) was highest at the TSS, diminishing with increasing distance from the TSS, as reported in other tissues[39,40,43] (Figure 2B). Motif analysis of target sites 1 kb upstream of the TSS revealed the majority of binding at promoter regions, with reduced binding at other genomic sites (Figure 2C). Transcription factor (TF) binding sites enriched in BMAL1 target regions included E-box, SP1, and hypoxia-inducible factor (HIF1) motifs (Figures 2D and S2B). Interestingly, while retinoic acid response elements (RREs), D-boxes, peroxisome proliferator activator alpha (PPARA), and BACH1 target sites were over-represented in liver ChIP-seq studies,[40] motifs belonging to myocyte enhancer factor 2 (Mef2), early growth response 2 (Egr2), neuronal Per-Arnt-Sim domain 2 (Npas2), sterol response element binding protein 1 (SREBP-1), and the homeobox TF Nkx2–5 are enriched in PVN BMAL1 target genes (Figure S2B). Peak visualization of BMAL1 target genes thyroid receptor alpha (*Thra*), and eukaryotic translation initiation factor 4A1 (*Eif4a*) revealed consistency in binding across biological replicates (Figures 2E and 2F). Functional enrichment analysis of BMAL1 targets identified pathways involved in circadian rhythms, glucocorticoid signaling, translation, and cellular metabolism (Figures 2G and S2C). Molecular function and reactome enrichment analysis highlighted genes corresponding to histone methyltransferase regulation, mitochondrial function, and nucleolar function (Figures 2H, 2I, S2D, and S2E). Interestingly, recent studies have shown BMAL1 to maintain specific functions in the nucleolus.[44] KEGG network analysis of ChIP-seq genes reveals an overlap of circadian genes with retrograde endocannabinoid signaling genes (Figure 2J). Network analysis highlights connections between circadian entrainment and regulation of glucocorticoid and steroid hormone receptor signaling pathways (Figure S2F). To determine whether ChIP-seq targets were bound rhythmically by BMAL1 *in vivo*, we performed ChIP-qPCR from enriched PVN tissue of male mice across the sleep-wake cycle and quantified gene expression of BMAL1-bound genes, including inositol 1,4,5-trisphosphate receptor type 2 (*Itpr2*), *Eif4a*, and *Dbp*. BMALl recruitment showed a trend for higher binding at ZT8 (Figure 2K), and Circacompare revealed rhythmic occupancy at both *Dbp* and *Eif4a1* (Figure S2G). These results highlight unique BMAL1 genomic targets involved in hormonal regulation and neuronal plasticity in the PVN.

## Single-cell transcriptomic analysis reveals highly divergent gene expression in specific PVN cell nuclei

While ChIP-seq revealed widespread genomic occupancy of BMAL1, we also utilized snRNA-seq, using PVN tissue from wild-type (WT) mice at ZT8 and ZT20, using two biological replicates per time point ($N = 5$ pooled PVN per biological replicate) (Figure 3A). We sequenced 30,109 nuclei and counted 28,360 genes (quality control steps are described

Author Manuscript Author Manuscript Author Manuscript Author Manuscript

in STAR Methods; Figures S3A–S3E). An average of 2,668 genes were detected per nuclei. We identified 34 clusters, grouped into 11 distinct cell types based on specific markers: glutamatergic neurons (*Slc17a6*), GABAergic neurons (*Slc32a1*), astrocytes (*Agt*), newly formed oligodendrocytes (*Mobp*, *Fyn*, and *Sirt2*), myelinating oligodendrocytes (*Mobp*), microglia (*Cx3cr1*), tanycytes (*Col23a1*), endothelial cells (*Cldn5*), pericytes (*Abcc9*), perivascular fibroblasts (*Slc47a1*), and vascular smooth muscle cells (*Mcam*) (Figures 3B, 3C, S3F, and S3G). Of sequenced nuclei, 12,750 were collected at ZT8 and 16,727 at ZT20 (Figure S3E). Most clusters showed broad representation from both ZT8 and ZT20 time points (Figure S3E). However, some clusters (such as clusters 0, “Glut-1,” and 1, “Glut-2”) were revealed at one ZT, underscoring the precise regulation of diurnal gene expression in the PVN (Figures 3B, 3C, and S3E). Cluster identities were largely consistent with published single-cell datasets of the SCN[45] and the whole and lateral hypothalamus.[46,47] Consistent with published data,[48] neurons were the most populous cell type, followed by oligodendrocytes and astrocytes (Figure 3D). Varying levels of nuclei from day and night composed each cluster, with some clusters (“Glut1–2”) having over 80% of their nuclei at one ZT (Figure 3E). PVN cell heterogeneity was preserved across time points and biological replicates (Figure S3D). To rule out potentially spurious results arising from variability across replicates, we adopted canonical correlation analysis (Seurat v.4[49]) to integrate the four samples using default parameters. Some clusters (for example, 0 and 1) remained different across samples even after batch correction. These clusters are identified as glutamatergic neurons, as indicated by *Slc17a6* expression. Heatmaps depict the top eight identifying marker genes in each cluster (Figure 3Fl Data 1). snRNA-seq data revealed diurnal expression of a wide range of neuropeptides or their signaling molecules, including *Oxt*, arginine vasopressin (*Avp*), *Thra*, and brain-derived neurotrophic factor (*Bdnf*) (Data 2). As expected, circadian genes such as *Clock*, *Bmal1*, and *Per3* are also expressed across the 34 clusters (Figure S3G). *Oxt* emerged as one of the genes with the highest diurnal variance in expression (Data 2). While the greatest expression of *Oxt* was observed in glutamatergic and GABAergic neurons, there was surprisingly high diurnal variance of *Oxt* in astrocytes and oligodendrocytes, suggesting additional roles for OXT in non-neuronal cells.

The PVN has been characterized by a majority of glutamatergic neurons and a minority of GABAergic neurons.[48,50] We identified 13 glutamatergic and five GABAergic clusters using *Slc17a6* and *Slc32a1* markers, respectively (Figures 4A, 4B, and S3F). *Slc17a6* and *Slc32a1*, involved in vesicular neurotransmitter release, showed distinct patterns in cell populations at ZT8 compared to ZT20 (Figure 4B). Greater heterogeneity in gene expression was observed across glutamatergic compared to GABAergic clusters (Figure S4C). To examine time-dependent changes within clusters, we examined differentially expressed genes (DEGs) between the ZTs. Glutamatergic clusters 7, 9, 10, 12, and 13 had many diurnally divergent DEGs (Figure S4D). Glut-4 shows a downregulation of nucleus-encoded mitochondrial genes at ZT8, suggesting diurnal changes in mitochondrial activity. However, some glutamatergic clusters showed very few diurnally expressed DEGs, suggesting unique roles of the circadian clock in certain PVN cell types (Figure S4D). GABAergic clusters also displayed varying amounts of diurnal DEGs, with GABA-3 and GABA-4 clusters showing higher numbers (Figure S4E). Produced by OXT receptor (Oxtr)-expressing PVN neurons, *Oxt* controls hunger in mice.[22,51] *Oxt* was the highest diurnally variant DEG in both glutamatergic and GABAergic clusters and expressed in multiple clusters (Figures 4C and S4F).

To study diurnal changes between neuronal subtypes, neurons were “pseudobulked” into a glutamatergic and a GABAergic cluster. Volcano plots of DEGs downregulated (blue) or upregulated (red) at ZT8 relative to ZT20 reveal many neuropeptide or neuropeptide precursors ($p < 0.05$) (Figure 4C). Gene Ontology revealed that both the glutamatergic and GABAergic clusters showed downregulation at ZT8 relative to ZT20 of genes involved in cellular metabolic processes and translation (Figures 4D and 4E). However, genes involved in neural projection and cell morphogenesis were upregulated in both neuron types. These results suggest that, depending on the time of day, PVN neurons may be engaged predominantly in cellular energetics, while, at other times, neurons re-organize and alter synaptic connections.

Importantly, certain diurnally invariant genes in neuronal clusters, such as Glut-13 and GABA-4, showed high expression and overlapped with genes identified in our BMAL1 ChIP-seq, suggesting that BMAL1 regulation occurred at these loci even though transcripts were not differentially expressed between ZTs (Supplemental Data S3). Pearson’s correlation coefficients were generated correlating ChIP-seq genes and diurnally expressed DEGs for “pseudobulked” neurons. This revealed a statistically significant positive correlation for both glutamatergic ($p = 0.0229$) and GABAergic ($p = 0.0491$) neurons (Figures S4G–S4F).

Astrocytes are important for maintaining SCN synchrony and rhythmic behavior.[38,52] Here, 25% of PVN cells were non-neuronal (Figures 3D and 4A), with astrocytes and oligodendrocytes being the most prominent (Figures 3D and S5A), and a similar number of cells were identified at both ZTs for these cells (Figure S5B). Two astrocytes (*Agt*-positive) and six myelinating oligodendrocytes (*Mobp*-positive) clusters were identified (Figure S5C). Non-neuronal cells also included microglia and one tanycyte cluster characterized by *Cx3cr1* and *Col23a1*, respectively (Figure S5D). Differential expression of ZT8 versus ZT20 transcripts in non-neuronal clusters reveals unique DEGs (Figures S5E–S5H). *Oxt* was also a DEG downregulated at ZT8 in Astrocyte-1 (Figure S5E). Although less is known about OXT in astrocytes, studies suggest that astrocytes engage in OXTR signaling.[53,54] While astrocyte clusters showed few diurnally variant DEGs, many transcripts overlapped with BMAL1-bound genes such as *Dbp*, *Nr1d1*, and *Nr1d2* (Data S3). These data suggest that the astrocyte clock may play a prominent role in PVN regulation of energy metabolism.

To interrogate additional diurnally expressed DEGs, we divided oligodendrocytes into “newly formed” (nf) and “myelinating” (m) subtypes (Figure S5F). DEGs in *nf*-oligodendrocytes, *m*-oligodendrocytes, and microglial clusters varied widely over ZTs, suggesting that these subtypes may have a prominent diurnal role in the PVN (Figures S5G–S5G). Of oligodendrocytes, nfOligos had the largest number of diurnal DEGs and diurnally invariant transcripts to overlap with the BMAL1 targets (Data 3). Astrocytes and *m*-oligodendrocytes were “pseudobulked,” revealing *Oxt* as a downregulated DEG at ZT8 for both cell types (Figure 4F). The overlap of BMAL1-ChIP-seq targets with diurnally

Author Manuscript Author Manuscript Author Manuscript Author Manuscript

variant astrocyte transcripts was the strongest positive correlation of all cell types tested ($R = 0.5074$, $p = 0.0019$); *m*-oligodendrocytes targets were only weakly correlated (Figures S5I and S5J).

Among microglia, which contribute to diet-induced obesity,[55] the microglia-3 cluster showed a high number of DEGs and the largest overlap of diurnally variant transcripts with BMAL1 ChIP-seq targets (Figure S5G; Data 3). We also examined tanycytes, nutrient-sensing radial glial cells projecting from the third ventricle.[56] Tanycytes display many more upregulated DEGs than downregulated DEGs at ZT8 relative to ZT20 (Figure S5H). Likewise, a larger number of BMAL1-ChIP-seq genes overlap with transcripts from tanycytes compared to other cell types (Supplemental Dataset 3). Finally, perivascular fibroblasts, endothelial cells, and vascular smooth muscle cells show pronounced changes in diurnal gene expression, which were also bound by BMAL1 (Figure S5H; Data 3).

Functional enrichment analysis of astrocyte "pseudobulked" DEGs reveals an upregulation of ion transport pathways at ZT8 relative to ZT20 (Figure 4G). During the nighttime, genes related to metabolism, phosphorylation, and translation were high compared to daytime (Figure 4G). In "pseudobulked" *m*-oligodendrocytes, DEGs upregulated at daytime correspond to cytoskeleton organization and cellular morphogenesis pathways (Figure 4H). *m*-oligodendrocyte genes involved in metabolism, phosphorylation, and translation pathways are also downregulated in the daytime (Figures 5G and 5H).

To further integrate snRNA-seq and ChIP-seq data, we utilized the Bayesian approach and platform to infer transcription factor activities, "BITFAM",[57] which infers TF activity (mapped in T-distributed Stochastic Neighbor Embedding plots; Figures S6A–S6C) from consensus sequences present in snRNA-seq transcripts and found in existing ChIP-seq datasets. Overlap of GABAergic and glutamatergic neuron clusters indicates similar TF regulation of diurnally variant genes. However, astrocytes and *m*-oligodendrocytes reflect very distinct transcriptional programming (Figure S6A). To identify the TFs that distinctly identify a cell type, we trained separate logistic regression models to identify the relevant TFs for glutamatergic and GABAergic neurons, astrocytes, and *m*-oligodendrocytes. Comparing the top five TFs for each major cell type, lack of overlap suggests that gene regulatory networks defining each cell type are specialized (Figure S6B).

To discern what TFs are potentially involved in cell-type-specific diurnal gene expression, another logistic regression model was trained on the TFs previously identified for each cell type. In the case of glutamatergic neurons, of the 31 TFs used previously to characterize that population, 20 were found to potentially regulate diurnal gene expression in glutamatergic neurons (Figure S6C). Certain TFs, like *Mef2*, also appeared in the motif enrichment analysis of this study, suggesting that BMAL1 and MEF2 may cooperate in driving diurnal PVN gene expression (Figure S6C).

To validate that diurnally variant DEGs that were also bound by BMAL1 are directly regulated by BMAL1, siBMAL1 was used to knock out BMAL1 expression in SH-SY5Y cells (Figure S7A). Normal and BMAL1-deficient cells were synchronized by serum shock and analyzed over subjective time for oscillations in BMAL1 target gene expression (Figure

Author Manuscript Author Manuscript Author Manuscript Author Manuscript

S7B). Expression of *Thra* and *Essra* genes, oscillated in control cells while displaying little to no expression in si*Bmal1* cells (Figure S7B). Not all genes were blunted by BMAL1 loss; *Eif4a1* showed increased expression at ST12 in the absence of BMAL1 compared to the control (Figures S7B and S7C), consistent with transrepression of CLOCK:BMAL1 targets, depending on their co-occupancy with other transcriptional regulators.[58] Rhythmicity was tested for all genes using the Jonckheere-Terpstra test (Figure S7C).

To further validate BMAL1-specific regulation of target genes in the PVN, we dissected PVNs from control and BMAL1-PVN KO mice at ZT8 and ZT20 and used flow cytometry to sort GFP-positive nuclei (Figure 5A). The AAV-GFP control virus showed poor localization of GFP to nuclei; thus, for the control (WT), all BMAL1-positive nuclei were collected. While GFP-injected control mice showed variation in *Per2* and *Essra* expression, a dampening of expression in BMAL1-deficient cells was observed (Figure 5B). *Dbp*, *Oxt*, and *Thra* expression followed similar trends in PVN BMAL-positive vs. BMAL-deficient nuclei (Figures 5B and S8A). Remarkably, while *Ox*t expression was highly diurnal in cells isolated from WT mice, considerable blunting of *Oxt* expression was observed in cells of BMAL1-deficient mice, and immunofluorescence revealed substantially less PVN OXT in the absence of BMAL1 (Figures 5C and 5D). OXT showed altered subcellular localization over time, being primarily localized to neuronal nuclei and somata at ZT8 and processes at ZT20 (Figure S8B). To determine whether diurnally variant hypothalamic OXT is reflected in serum, we analyzed serum OXT. Serum OXT showed a 24-h rhythm, peaking at the end of the feeding phase (ZT0) and reaching its nadir during the late resting phase (JTK_Cycle; $p = 9.16e-9$) (Figure 5E). Importantly, loss of PVN BMAL1 resulted in diurnal changes in serum OXT, indicating that PVN BMAL1 expression is necessary for normal diurnal patters of OXT in the circulation (Figure 5F).

Finally, to determine whether altered OXT levels might contribute to the arrhythmic phenotypes of PVN BMAL1-KO mice, we injected PVN BMAL1-KO mice peripherally once daily for 16 days with saline or OXT[59] at the peak time of serum OXT concentration (Figure 5G). Bodyweight did not significantly change between groups (Figure S8C); however, home cage locomotion patterns were improved by daily OXT administration (Figures 5H, S8D, and S8E). OXT administration peripherally was sufficient to raise serum OXT for at least 1 h following injection (Figure 5I), and total average activity per day was increased by OXT injections (Figure 5J). Although the average difference between night and day activity was not significantly different in the OXT-injected mice compared to controls (Figure 5K), the average night activity was significantly greater than the average daytime activity in OXT-injected mice (Figure S8F). OXT injections did not acutely change locomotion, as revealed by activity 1 h before, during, and after the injection hour compared to control-injected mice (Figures S8G and S8H). In addition to an improved activity rhythms in OXT-injected BMAL1-PVN KO mice, average total food intake across 24 h was decreased (Figures 5L and S8I), consistent with the anorectic effect of OXT.[60] Average food intake during the night versus day showed only a trend of higher nighttime food consumption in the OXT-injected mice compared to daytime food consumption (Figures 5M and S8J). Decreased food intake 1 h following OXT injection was observed (Figure S8K). Peripherally administered OXT has been shown to induce PVN activity and subsequent induction of OXT.[59] To test whether OXT injections were effective in activating the PVN

Author Manuscript

Author Manuscript

Author Manuscript

Author Manuscript

of PVN BMAL1-KO, the PVN of saline- and OXT-injected mice was analyzed for c-FOS activation. OXT induced c-FOS in the PVN compared to saline (Figures 5N and S8L). As OXT has recently been shown to be involved in the regulation of lipolysis,[61] a subset of mice was tested for changes in circulating free fatty acids (FFAs). Though there was a slight trend of increased circulating FFA in OXT-injected mice; it was not significant at the collection time points (Figure S8M).

## DISCUSSION

In this study, we reveal that loss of BMAL1 in the PVN of mice results in disruption of energy expenditure and food intake rhythms and a loss of entrainment to normal light/dark conditions, which coincides with altered peripheral tissue rhythmicity. Though the SCN contributes to organism-wide rhythms, data point to the strong role of the circadian clock in extra-SCN hypothalamic nuclei in driving organism-wide changes in circadian physiology.[18,19] It is striking that inducible BMAL1 loss in the PVN results in arrhythmic behavior, considering constitutive loss of BMAL1 in the SCN does not eliminate rhythmicity in entrained conditions.[34] However, what may be compensation by other proteins in the SCN has also been noted in the PVN, where *Sim1*-specific loss of BMAL1 from birth also does not result in arrhythmicity.[19] Here, we reveal widespread genomic occupancy by BMAL1 in the PVN at genes important for synaptic plasticity. In conjunction with snRNA-seq at antiphase time points, these data show that many diurnally variant genes are BMAL1 regulated and that BMAL1 contributes to cell-type-specific regulation of gene expression in the PVN over the day/night cycle. As a region of the brain important for physiological homeostasis, including regulation of energy intake and expenditure, our findings implicate circadian regulation of these processes through a wide range of cell types.

Little is known about BMAL1's function in the PVN or the mechanisms by which it contributes to reduced diurnal rhythms. However, other clock proteins in the hypothalamus, such as REV-ERBα and REV-ERBβ, have been shown to regulate diurnal leptin sensitivity and rhythmic energy intake.[21] One of the striking phenotypes associated with BMAL1 loss in the PVN is the arrhythmic activity and disrupted energy intake patterns that ensue following KO of BMAL1. To our knowledge, no other non-SCN tissue-specific deletion of BMAL1 results in arrhythmic activity in entrained conditions. Rather, loss of locomotor rhythms is usually revealed in free running (constant dark) conditions, even in the context of circadian mutant mice.[62–65] Our study addresses both the extent to which food can serve as a zeitgeber in the BMAL1-PVN KO mice and the maintenance of light responsiveness in the SCN. In this model, restricted energy intake was not only sufficient to partially overcome the arrhythmic behavior of the mice, it partially counteracted peripheral changes in diurnal gene expression resulting from the loss of BMAL1 in the PVN. Although there are no known direct PVN projections to the SCN, the PVN projects to other hypothalamic nuclei, some of which project to the SCN. Like WT mice exposed to light during free running conditions,[66] we were able to observe light-induced expression of c-Fos in the SCN in BMAL1-PVN KO mice. However, *Per2* rhythms in the SCN of BMAL1-PVN KO were antiphase, suggesting that lack of entrainment could be partially SCN dependent.

Author Manuscript Author Manuscript Author Manuscript Author Manuscript

While genomic organization of BMAL1 has been studied extensively in some contexts,[18,40,67,68] less is known about BMAL1 targets in the CNS. Based on studies showing a relatively consolidated phase of BMAL1 expression across tissues *in vivo*[69] as well as our own PVN ChIP-qPCR (Figure 2K), we considered ZT8 as the optimal time point for capturing peak BMAL1 binding in the PVN. However, studies have shown circadian gene expression to be cell type specific, and even in the context of the SCN, single-cell sequencing approaches have revealed some level of cell specificity in circadian gene expression.[45,46] Similarly, the PVN snRNA-seq data also show heterogeneity in diurnal gene expression within subclusters of major cell types. For example, the glutamatergic neuron clusters Glut-1 and Glut-2 show a completely divergent pattern of diurnal gene expression, with Glut-1 poorly represented at the ZT8 time point and Glut-2 poorly represented at ZT20. In many cases, diurnally invariant genes were also BMAL1 targets in the PVN. For example, many astrocyte genes that were diurnally invariant were also bound by BMAL1 in ChIP-seq analysis. This could be due to the fact that, though BMAL1 binding is greatest during the late resting period, snRNA-seq was performed at this same time. Thus, some genes activated by BMAL1 may not show elevated transcript expression until several hours later. Other studies have revealed that, though binding of the CLOCK:BMAL1 heterodimer to chromatin is highly rhythmic, transcriptional output is heterogeneous, as expression relies on binding of tissue- and context-specific cofactors.[70,71]

Only recently was BMAL1 shown to be important in oligodendrocytes for oligodendrocyte-mediated myelination and sleep regulation.[72] In addition to oligodendrocytes, our results reveal that microglia have many diurnal DEGs, suggesting an important role for the microglial clock in the PVN. Activation of these immune cells can drive inflammation, energy intake, and weight gain.[55,73]

Interestingly, snRNA-seq analysis of the young vs. aged female hypothalamus underscores the loss of *Oxt* expression in aged mice,[74] and a similar blunting of OXT signaling occurs in aged male mice.[75] Circadian robustness generally is damped during aging, with decreased circadian amplitude for the sleep/wake cycle,[76] SCN firing,[77] body temperature, melatonin, and cortisol (reviewed in Hood and Amir[78]). The strong diurnal variance in *Oxt* expression may ultimately be diminished in the process of aging. The *Oxt* locus has been shown as a BMAL1 target in ChIP-seq of other tissues,[39] and PVN BMAL1 loss reduced *Oxt* expression and secretion (Figure 5). While *Sim1*-Cre deletion of BMAL1 has been shown to reduce expression of arginine vasopressin (*Avp*) in the PVN, expression of PVN *Oxt* was not significantly altered in that study.[79] However, our results reveal that *Oxt* expression is highly diurnal in many different cells types, which could explain the rhythmic presence of *Oxt* in WT mice and loss of diurnal gene expression changes in the context of BMAL1 deletion. A growing body of literature supports a role for OXT in feeding and metabolism[80] and adipose tissue lipolysis,[61] and a high-fat diet diminishes the rhythmicity of OXT.[81] Our data suggest that the PVN clock regulates rhythms in circadian physiology in part by modulating OXT in the PVN, as peripheral OXT administration improved behavioral rhythmicity, reduced energy intake, and induced activation of c-FOS in the PVN of BMAL1-PVN KO mice.

Interestingly, whole-hypothalamus snRNA-seq around the 24-h cycle has revealed that gene expression rhythms are generally lost throughout aging,[82] including HIF1a and senescence-

Author Manuscript

Author Manuscript

Author Manuscript

Author Manuscript

regulatory pathways. HIF1 motifs were highly represented in our BMAL1 ChIP-seq, suggesting that a decline in clock function correlates with the loss of HIF1a activity throughout aging. Our data are consistent with a robust clock in the PVN, which drives rhythms at the organism-wide level. However, we reveal pronounced cell-type-specific patterns of gene expression in this region, which will hopefully assist in future studies addressing cell-type-specific functions of the PVN in regulating diurnal behavior and circadian metabolism.

Collectively, our data unveil a highly dynamic circadian clock in specific cells of the PVN, which is controlled in part by BMAL1. This dynamic PVN clock contributes to body-wide rhythmicity, in part by controlling the robustness of OXT secretion, underscoring its critical role in metabolic health. BMAL1 function in the PVN promotes diurnal gene expression of genes involved in neuroendocrine regulation and controls pathways central to cell function, including chromatin and mitochondrial regulation.

## Limitations of the study

Limitations of our study include the use of only antiphase time points for assessing diurnal gene expression in the PVN via snRNA-seq rather than a higher-resolution circadian profiling. The latter could certainly reveal a much larger number of genes potentially involved in maintenance of behavioral rhythms. An additional confounding factor and limitation of our study pertains to the ChIP-seq and snRNA-seq experiments, where enriched PVN tissue was used, which may account for the slightly higher-than-expected number of tanycytes in our snRNA-seq, for example. However, the annotated cellular populations and their quantities in our PVN snRNA-seq analysis are generally consistent with prior studies analyzing PVN cell populations.[48,50] Finally, a primary limitation of our study is that, though the SCN remains light responsive in BMAL1-PVN KO mice, the data from this study cannot rule out that loss of PVN BMAL1 does not alter SCN function. In fact, gene expression data show that, while the SCN remained light responsive, diurnal expression of *Per2* was abnormal. As indirect projections exist between the PVN and the SCN, whether SCN rhythmicity is affected in these mice will be an important determination. Furthermore, OXT could be restoring behavioral rhythmicity in part by indirect action at the level of the SCN. The independence (or lack thereof) of the PVN and SCN clocks will be an important next step in understanding the role of BMAL1 in the PVN on rhythmic behavior.

# STAR★METHODS

## RESOURCE AVAILABILITY

**Lead contact—**Further information and requests for resources and reagents should be directed to and will be fulfilled by the lead contact, Kristin Eckel-Mahan (Kristin.l.Mahan@uth.tmc.edu)

**Materials availability—**This study did not generate new unique reagents.

Author Manuscript Author Manuscript Author Manuscript Author Manuscript

**Data and code availability—**The structured data and code availability statement consists of three bulleted sections. Each section must be present. A template for the data and code availability statement can be found here: https://www.cell.com/star-authors-guide.

- ChIP-sequencing data and snRNA-seq data have been deposited in the Gene Expression Omnibus (GEO) repository under the accession number GEO: GSE231940 and GSE231734.
- This paper does not report original code.
- Any additional information required to reanalyze the data reported in this work paper is available from the lead contact upon request.

## EXPERIMENTAL MODEL AND STUDY PARTICIPANT DETAILS

Mice were housed at the Brown Foundation Institute of Molecular Medicine in accordance with Institutional Animal Care and Use Committee (IACUC). Mice were housed at 21°C–22°C with a standard 7a.m.−7p.m. (12:12h) light dark cycles with a standard pellet chow (13% kcal from fat, LabDiet #5R53). Unless otherwise indicated, mice were allowed to drink and eat *ad libitum*. Animal care and procedures were approved by the University of Texas Health Science Center at Houston Institutional Animal Care and Use Committee. For all experiments, *zeitgeber* (ZT) 0 refers to light onset in the room, corresponding to the beginning of the animals' sleep/fasting phase. ZT12 refers to the onset of darkness, the beginning of the animals' active/feeding phase. C57Bl6 mice were obtained from the Jackson Laboratory. $Bmal1^{flox/flox}$ mice were obtained from the Qingchun Tong Lab. Body weight was recorded weekly. Genotyping for $Bmal1^{flox/flox}$ mice was carried out as described (Kim et al., 2020).

## METHOD DETAILS

**Stereotaxic surgery and viral constructs—**Adult male and female mice were placed on a stereotaxic frame (David Kopf Instruments) under the anesthetized condition with Ketamine + Xylazine (100 mg/kg + 10 mg/kg). AAVDJ8-CMV-GFP and AAV5-CMV-CRE-GFP vectors used as previously reported.[14] Viral vectors were delivered through a 0.5 μL syringe (Neuros Model 7000.5 kH, point style 3; Hamilton, Reno, NV, USA) mounted on a stereotaxic injector (Quintessential Sterotaxic Injector, Stoelting, Wood Dale, IL, USA) at a rate of 40 nL/min. Viral preparations were tittered at ~1012 particle/mL. The vectors were sterotaxically injected into the bilateral PVN (150 nL per side) with the following coordinates: AP: −0.5 mm, ML: +/− 0.25 mm, DV: −4.8 mm. Mice were administered Carprofen (5 mg/kg) for three day following surgery and allowed to recover for a week, after which they were used for experiments. AAV-GFP injected mice were used as a control group.

**Immunostaining and quantification—**For immunostaining and to validate viral injection PVN specificity, mice were transcardially perfused with 0.9% saline buffer followed by 10% neutral buffer formalin (NBF). The brains were post-fixed in 10% NBF at 4°C overnight and then cryoprotected in 30% sucrose in 1XPBS for two days. The brains were sectioned at 30 μm on a sliding microtome (Leica Biosystems) and processed

Author Manuscript Author Manuscript Author Manuscript Author Manuscript

with routine immunohistochemistry. In brief, the free-floating slices were rinsed with 1XPBS and incubated with blocking buffer (3% BSA, 0.3% Triton X-100 in PBS) for 1 h at room temperature (RT) to reduce nonspecific antibody binding and increase antibody penetration. The sections were then incubated with primary antibody in blocking buffer at 4C overnight. Primary antibody BMAL1 (1:200, NB100–2288, Novus Biologicals), c-Fos (1:1000, #2250, Cell Signaling Technology) and OXT (1:200, #AB911, Millipore) were used. The brain sections were washed with 1XPBS and incubated with secondary antibody (DAPI, 1:10,000, AlexaFlour 555 goat anti-rabbit 1:200, #A21430, Invitrogen, AlexaFlour 555 donkey anti-mouse 1:200, #A21430 and Invitrogen Donkey anti-goat AlexaFlour Plus 594, 1:200, #A32758) in blocking buffer for 2h at RT. The signal was captured and imaged with a Nikon AX-R confocal microscope (Nikon).

For c-FOS counting, sections that contain the SCN at matched anteroposterior levels were chosen from each mouse. Within the SCN boundary, all c-FOS positive cells with bright and clear oval nuclei profiles were counted under the fluorescent microscope with the 20x objective at 2x zoom. The number from all sections were averaged and analyzed in all animals. The same process was repeated for c-FOS, BMAL1 and OXT quantification in the PVN.

**Diurnal behavior recording—**For diurnal behavioral recording, mice were single housed in cages containing infrared sensors (STARR Life Sciences, PA) to monitor total home cage diurnal activity. Data were collected using VitalView (STARR Life Sciences) and locomotion data were analyzed using ClockLabs software (ActiMetrics, IL).

**Phenomaster metabolic cage recording—**Food intake and locomotion activity levels were measured using indirect calorimetry. Mice were single housed in Phenomaster (TSE Systems-USA) cages. Mice were given *ad libitum* access to normal chow food and water and were acclimatized in the chamber for at least 2 days prior to data collection. Each cage was measured every 39 min. Measurements of feeding and locomotion were collected continuously during the whole measurement period. Data were prepared by averaging the total 24 hr, or by averaging the day (12 h) and night (12 h) periods (12hr).

**Oxytocin injections—**Oxytocin (Abcam #ab120186) was prepared in sterile 0.9% saline and delivered via intraperitoneal injections at 1 mg/kg in BMAL1-PVN KO mice at ZT0 (onset of light phase). Injections were conducted daily for up to 16 consecutive days. For control, a cohort of BMAL1-PVN KO mice were injected daily with sterile 0.9% saline rather than OXT.

### Cell culture experiments

**Cell culture:** SH-SY5Y cells were obtained from the Sheng Zhang lab and cultured in Eagle’s Minimum Essential medium (EMEM) supplemented with 10% fetal bovine serum, 100 units ml−1 penicillin G sodium, and 100 µg mL−1 streptomycin.

**Si-Knockdown:** Cells seeded at $2 \times 10^5$ cells/cm$^2$ and then harvested at 80% confluency for transfection with the Amaxa Cell Line Nucleofector Kit V (#VCA-1003, Lonza). The cells were electroporated using a single square-wave pulse of 200V with a duration of

Author Manuscript Author Manuscript Author Manuscript Author Manuscript

20 ms (Gene Pulser Xcell #1652660, BioRad). Cells were transfected with 30 pmol of siRNA. Knockdown was performed using mouse *Silencer* Select *Bmal1* siRNA (Ambion # 4390843). Scrambled siRNA with similar GC content served as control. Cells were immediately replated following electroporation.

***Serum Shock.:*** At 80% confluence (ZT0) the cells were re-fed with EMEM supplemented with 50% horse serum (serum shock). After 2 h in serum-rich media, cells were rinsed and re-fed with serum-free EMEM. At 12 h (ZT12) from the serum treatment (ZT0), cells were harvested at the indicated times (every 6h over a 48h period) dishes were washed with ice-cold PBS, lysed, and harvested in 1 mL TRIzol reagent by scraping with a rubber scrapper and RNA extracted from cell lysates.

**Immunoblotting—**Cultured cells were sonicated (Qsonica, Newton, USA) for 10 s at 30% amplitude in RIPA lysis buffer. Samples were spun at 10,000× *g* for 10 min to eliminate insoluble material. The total protein levels of the lysates were determined using the bicinchoninic acid method. Protein extracts were analyzed using 8% sodium dodecyl sulfate polyacrylamide gel electrophoresis followed by transfer to the nitrocellulose membrane before staining with primary antibodies of either BMAL1 (1:1000, ab93806, Abcam) or ACTIN (1:1000, ab119716, Abcam). Secondary antibodies conjugated to horseradish peroxidase and enhanced chemiluminescence substrate were used for detection.

**RNA extraction and qRT-PCR—**Total RNA was isolated using TRIzol reagent according to the manufacturer’s protocol (Thermo Fisher Scientific). One μg of total RNA was used for cDNA synthesis using an iScript cDNA Synthesis Kit (Bio-Rad). Advanced Universal SYBR Green Super mix (Bio-Rad) was used for qPCR amplification using a Bio-Rad C1000. PCR protocol settings were as follows: 95°C for 30 s, 95°C for 10 s, 62°C for 30 s, and then 39 cycles at 65°C for 31 s and 65°C for 5 s. Ribosomal subunit 18S expression was used as normalization for gene expression. Fold change in mRNA expression for each gene was calculated using 2−ΔΔC. For multiple time point experiments, expression is normalized to the control condition at ZT8 or in the case of serum shock, ZT0.

**Chromatin immunoprecipitation—**Chromatin Immunoprecipitation was carried out using the Cell Signal kit according to the protocol. Dissected PVN tissues were weighed pooled for 100 mg of tissue per sample. The pooled tissue was then added to PBS with protease inhibitor cocktail (PIC) into a dish on ice and minced with scissors. The minced tissue was crosslinked with 1.5% formaldehyde in PBS + PIC for 10 min on a rocker at room temperature. Crosslinking was quenched with 1.25 mM glycine (rocked for 5 min) and then centrifuged (5 min, 500g, 4C). The pellets were washed once with ice-cold 1XPBS before being resuspended in PBS with PIC. The pellets were homogenized using glass douncers (2 mL), 25–30 strokes, and incubated on ice for 30 min. The cell suspension was centrifuged at 2,000g for 5 min at 4C. Following this, the supernatant was removed and cells were resuspended in ice-cold Buffer A + DTT + PIC and incubated on ice for 10 min. Tubes were inverted every 3 min to mix. Nuclei were pelleted by centrifugation (2000g, 5 min, 4C). Supernatant was discarded and the pellet was resuspended in ice-cold Buffer B + DTT + PIC. Nuclei were pelleted by centrifugation (2000g, 5 min, 4C) and

Author Manuscript

Author Manuscript

Author Manuscript

Author Manuscript

then resuspended in Buffer B + DTT + PIC. Microccal Nuclease #10011 was added to each sample. Samples were incubated for 20 min at 37C with mixing by inversion every 3–5 min. Enzymatic digestion was stopped by adding EDTA #7011 to each sample and placing the samples on ice for 1–2 min. Samples were pelleted by centrifugation (16,000g, 1 min, 4C). Nuclear pellets were resuspended in ChIP Buffer + PIC and incubated on ice for 10 min. Each sample was sonicated on ice (5 s/25 s ON/OFF, 1.5 min, 30% Amp) to break the nuclear membranes. Lysates were clarified by centrifugation (9,400g, 10 min, 4C). Each supernatant was diluted in ChIP Buffer + PIC. 10uL was removed from each sample and stored in 4C to serve as the 2% Input. BMAL1 antibody (ab93806, Abcam) was added to replicates 1 & 2 while Rabbit IgG #2729P was added to the negative control. Samples were incubated overnight on a rotator at 4C. The following day, ChIP-Grade Protein G Magnetic Beads #9006 were added to each sample and incubated for 2h at 4C on a rotator. Each sample's beads were pelleted by placing the sample tubes on a magnetic separation rack #7017. Supernatant was discarded and the beads were then incubated with low salt wash buffer (5 min, 4C) on a rotator followed by pelleting beads with the magnetic rack and discarding the supernatant. This was repeated two more times with low salt wash buffer followed by a high salt wash buffer. Next ChIP Elution Buffer was added to the 2% inputs and each sample's beads. Samples were incubated for 30 min at 65C with gentle vortexing (1200 rpm) and then beads were pelleted with the magnetic rack and the eluted chromatin supernatant was collected. All samples including input were reverse cross linked by adding NaCl and Proteinase K #10012 and incubated for 2h at 65C. For DNA purification, DNA Binding Buffer #10007 was added to each sample. Samples were then placed in a DNA spin column with a collection tube and centrifuged (18,500g, 30 s, RT) followed by discarding the collection tube liquid at the end. DNA Wash Buffer #10008 was added to each DNA spin column and the columns were centrifuged (18,500g, 30 s, RT) followed by discarding the collection tube liquid at the end. DNA was eluted by adding DNA Elution Buffer #10009 followed centrifugation (18,500g, 30 s, RT) into new collection tubes.

### Single nuclei isolation

**Tissue dissection:** Single nuclei isolation for the single nuclei RNA-seq analysis was performed on five pooled PVN tissues dissected from male C57Bl6 mice aged 10–12 weeks at two time points, ZT8 and ZT20. PVNs were dissected from 10 to 12 weeks old male Bmal1-PVN KO mice two weeks following AAV-CRE-GFP injection. Male C57bl6 mice 10–12 weeks old served as controls. Mice scarified during the dark phase, at ZT20, were kept in complete dark during the dissection. Mice were sacrificed using CO2. Brains were quickly dissected and then transferred to a 0.5mm stainless steel coronal brain matrice (Kent Scientific) on ice where they were sectioned with a razor blade. A coronal section (approximately −0.3 mm bregma to −1.0 mm bregma) was obtained and placed in ice-cold artificial cerebral spinal fluid (aCSF) while the PVN region was excised using a 0.75 mm diameter micro punch (Braintree Scientific). The PVNs were flash frozen in liquid nitrogen and stored in −80C until further use.

**Nuclei isolation:** Five PVNs were pooled for each sample. PVNs were homogenized in a glass douncer (2mL) in lysis buffer (320 mM D-Sucrose, 5 mM $CaCl_2$, 3 mM $Mg(Ac)_2$, 10 mM Tris, 0.1 mM EDTA, 0.1% NP40, 0.1 mM PIC, 1 mM β-Mercaptoethanol) and RNase

Author Manuscript

Author Manuscript

Author Manuscript

Author Manuscript

inhibitor on ice. The homogenized tissue was filtered through a cell strainer (12 × 75 mm) and then added to an upper gradient buffer (5 mM $CaCl_2$, 3 mM $Mg(Ac)_2$, 10 mM Tris, 0.1 mM PIC, 1 mM β-Mercaptoethanol, 50% 60% OptiPrep Gradient). The mixture was inverted a few times and then added on top of 10 mLs of lower gradient buffer (29% 60% OptiPrep Gradient) in a 3 ½ Beckman centrifuge tube. The tube was centrifuged at 7500 rpm for 30 min at 4C. The contents were decanted and the pellet was resuspended in 1xPBS with RNase inhibitor. The nuclei were filtered through a cell strainer (12 × 75 mm) and then imaged under a microscope to check debris and nuclei morphology.

**Flow assisted cell sorting—**Following validation of intact nuclei with minimal debris, the samples were kept on ice. Nuclei were sorted on a special-order BD FACSAriaII cell sorter using a 100 μm nozzle and purity mode. Gating strategy to isolate single GFP+ or GFP- nuclei was as follows: nuclei versus debris (forward scatter (FSC) area vs. side scatter (SSC) area, singlets (SSC-W vs. SSC-A followed by FSC-H vs. FSC-A), and finally autofluorescence (ex. 405 nm/emission filter 610/20 versus GFP (ex. 488 nm, emission filter 530/30). Buffered blood bank saline (Thermo Scientific) was used as a sheath fluid and the nuclei were sorted into 300 μL of 1XPBS.

**Blood collection—**At day and night time points, 100–500μL of blood from mice was collected via submandipbular bleeds. Blood was collected in 1.5uL microcentrifuge tubes with 5uL of 0.5M chilled EDTA and Aprotinin (500 KIU/mL of blood) on ice. Serum was isolated by spinning blood down at 4,800g for 10 min at 4C and then stored in −80 C.

**Oxytocin ELISA—**To avoid matrix interference, OXT extraction was carried out on serum using 200 mg C18 Sep-Pak columns washed with 0/1% trifluoroacetic acid (TFA) and then equilibrated with acetonitrile per the Oxytocin ELISA Kit (Enzo Life Sciences #ADI-900–153A) protocol. Elution was carried out with 95% acetonitrile and 5% 0.1% TFA followed by evaporation to dryness using a rotovac. The extracted OXT was reconstituted in Assay Buffer and stored in −80C until further use. The EILSA was performed by the Oxytocin ELISA Kit protocol. The samples, standards and controls were set up according to the protocol. The plate was incubated at 4C overnight for 18–24h followed by 3 washes with the wash buffer. The pNpp solution was added to each well followed by a 1h incubation at RT. Immediately following the incubation, the stop solution was added and the plate was read at 405nm in the Cytation 5. To normalize to the blanks, the average blank OD value was manually subtracted from the sample absorbance OD values. The OXT concentration was interpolated from fitting the standards’ OD values to a four-parameter logistic curve in GraphPad.

**Free fatty acid ELISA—**Plasma free fatty acid (FFA) were measured with EnzyChrom Free Fatty Assay Kit (BioAssay System, cat no. EFFA-100). The standards and samples were set up according to the protocol. After adding the required reagents, the plate was incubated at room temperature for 30 min and then read at 570nm. The FFA concentration was calculated from fitting the standards’ OD values to a standard curve.

**ChIP-sequencing library preparation—**The purified and fragmented DNA samples were submitted to Cancer Genomics Center at The University of Texas Health Science

Author Manuscript

Author Manuscript

Author Manuscript

Author Manuscript

Center at Houston (CPRIT RP180734). The 100bp-300bp DNA fragments were selected by Kapa Pure Beads (#7983280001, Roche Holding AG), which were used for library preparation. The libraries were prepared following the protocol of KAPA Hyper Prep Kit (KK8502, Roche Holding AG). Briefly, the fragmented DNAs were repaired both ends, and an adenine (A) was added to the repaired ends. This end-repair and A-tailing procedure was performed at 20°C for 30 min followed by 65°C for 30 min. Then, the adapters with unique indexes, which can identify each sample during sequencing, were ligated to both ends of each fragmented DNA. After ligation, the DNA fragments with adapters were cleaned up by magnet beads. The proper sizes of DNA fragments were selected. The selected DNA fragments were quantified by quantitative polymerase chain reaction (qPCR) and amplified by Bio-Rad C1000 Touch Thermal Cycler (Bio-Rad Laboratories). The final library was qualified by Agilent Bioanalyzer 2100 (Agilent Technologies) and quantified by qPCR. The libraries were pooled and subjected to a paired-end 75-cycle sequencing on an Illumina NextSeq 550 System using High Output Kit v2.5 (#20024907, Illumina, Inc.).

**ChIP-sequencing analysis—**ChIP-Seq of BMAL1 in the PVN was performed on the Illumina platform. All reads were mapped to the mm10 reference genome using Bowtie2, and only unique mapped reads were used for subsequent analysis. ChIP-seq peaks were called using MACS2 at default thresholds. The called peaks with q value (FDR) < 0.05 and fold-enrichment >2 were annotated with gene names. These filtered peaks lying within 5 kb upstream of the transcription start site (TSS) of a gene or within its gene body were retained for peak annotation. The Integrative Genomics Viewer (IGV)[88]) was used to visualize *Per2 and Itpr2*. Peak annotation, visualization and distribution of the transcription factor binding loco relative to the TSS was conducted using ChIPseeker.[89] Hypergeometric Optimization of Motif EnRichment (HOMER)[90] was used for motif analysis. Gene enrichment analysis was performed using ShinyGO.[96] The Gene Ontology, molecular functions, reactome and KEGG databases were used. Pathways containing between 5 and 2000 genes were retained.

### Single-nuclei RNA-Sequencing analysis

**Library preparation:** The isolated nuclei were submitted to UTHealth Cancer Genomics Core at The University of Texas Health Science Center at Houston (CPRIT RP180734). The single nuclei capture and library construction were performed by following the Chromium Single Cell 3′ Reagent Kits v3.1 protocol (CG000204). Briefly, cells were resuspended in PBS with 0.04% BSA and RNase inhibitor at a concentration of 700–1200 cells/μL. The single nuclei were loaded onto Chromium Next GEM Chip G (PN-1000120) with partitioning oil and barcoded singe cell gel beads. The barcoded and full-length cDNA is produced after incubation of the gel beads-in-emulsion (GEMs) and amplified via PCR for library construction. The library preparation is performed by following the protocol of Chromium Single Cell 3′ GEM, Library & Gel Bead Kit v3 (PN-1000121). The quality of the final libraries was examined using Agilent High Sensitive DNA Kit (#5067–4626) by Agilent Bioanalyzer 2100 (Agilent Technologies, Santa Clara, USA). The libraries were sent for the paired-end sequencing on an Illumina Novaseq System (Illumina, Inc., USA).

**Single nuclei RNA-Sequencing analysis:** The Cell Ranger Single Cell Software Suite (v7.0.0) was used to perform bioinformatics analysis. The reads were aligned to the mouse

Author Manuscript Author Manuscript Author Manuscript Author Manuscript

transcriptome reference (mm10, Ensembl 93) with STAR [cite: 23104886] with including introns model. Raw read count tables were analyzed using the Seurat (v4.1.0) [49] standard pipeline on the R platform (v4.1.1). DoubletFinder[93] was used to remove the potential doublets using with a doublet rate # (Number of cell)/500*0.4/100 for each sample. FindVariableGenes function was used to calculate the principal components. Cell clusters were identified using the shared nearest neighbor algorithm with a resolution parameter of 0.8. UMAP clusters of cells were identified based on the first ten principal components. FindMarkers function was used to identify differentially expressed genes between cell groups using Wilcoxon Rank-Sum test. Feature plots and Violin plots were displayed with the log (raw read count +1) of the gene/cell on UMAP embedding.

**“Pseudobulk” differential gene expression analysis:** For differentially expressed genes, cells corresponding to samples at ZT8 and ZT20 were grouped within each cellular population of PVN cells (such as *Slc17a6* and *Slc32a1*). Genes with altered expression upon were then identified within the PVN cell population accounting for averaged expression differences. Wilcoxon test from the Seurat v3[97] analysis pipeline was used to identify significant gene expression changes (FDR <0.05) within each category of PVN cells instead of identified cellular clusters. Gene enrichment analysis was performed using ShinyGO.[96] The Gene Ontology database was used. Pathways containing between 5 and 2000 genes were retained.

**BITFAM analysis and logistic regression classifier:** The inferred transcription factor (TF) activities of each nuclei was calculated using the Bayesian inference transcription factor activity modeling (BITFAM) algorithm (v1.0) implemented in R with standard settings (Gao et al., 2021).[57] BITFAM results were first visualized as a t-SNE using the Rtsne R package (v0.15). The count matrices for the Seurat objects and BITFAM results were exported from R for use in Python. To determine the TFs most useful in distinguishing cell types, a logistic regression classifier was trained in Python with the scikit-learn package with balanced class weighting and L1 regularizer. Overfitting was avoided through a train/test split of 80/20 where test accuracies were >90%. The TFs were ordered based on magnitude of trained logistic regression coefficients. Cluster IDs were used to create a heatmap of the top five TFs by coefficient and their inferred activity for each of the four major cell types. To determine the TFs important for distinguishing ZT8 or ZT20, the above procedure was repeated, however training features were limited to the TFs that were previously identified for each of the four major cell types.

## QUANTIFICATION AND STATISTICAL ANALYSIS

Initial data were collected in Microsoft Excel 2021. GraphPad Prism 8.0 (GraphPad Software, Inc., La Jolla, CA, USA) was used for all statistical analyses and construction of graphs. Data are shown as mean with SEM. Significance ($*p < 0.05$, $**p < 0.01$, $***p < 0.001$, $****p < 0.0001$) was determined by t-tests or for experiments involving more than one variable, significance was assessed using two-way ANOVA followed by tukey’s post hoc test, as indicated in the figure legends. Data points that exceeded a predetermined 1.5 standard deviation from the mean were considered outliers. For experiments assessing rhythmicity, we used both the JTK_Cycle non-parametric test[94] and cosinor analysis.

Author Manuscript

Author Manuscript

Author Manuscript

Author Manuscript

JTK_Cycle (R Studio)[94] was applied, using a window of 20–28 h to capture diurnal oscillations. For serum shock experiments, rhythmicity was ascertained from all values excluding the ZT0 (unsynchronized) time point. To calculate if variables fit to the cosinor model, we performed cosinor regression in R studio with the packages "cosinor" to calculate rhythm $p$-value, mesor and amplitude. For the ChIP-qPCR samples, CircaCompare (Parsons et al., 2019)[95] was used to evaluate rhythmicity.

### ADDITIONAL RESOURCES

No additional resources

## Supplementary Material

Refer to Web version on PubMed Central for supplementary material.

## ACKNOWLEDGMENTS

We would like to thank Dr. Sheng Zhang for providing the SH-SY5Y cells. We thank Dr. Robin Work, Cneshia Taylor, and Nastassia Mason for help with animal care and husbandry and Dr. Mao Zhengmei for assistance with confocal imaging. This study was supported by NIH grants R01DK114037 (to K.E.-M.), R01DK125922 (to K.E.-M.), F31DK132895–01 (to R.V.D.), NIH R01 DK136284 (to Q.T.), and R01 DK131446 (to Q.T.) and the John J. Kopchick Research Award (to R.V.D.). Sequencing data were generated by the UTHealth Cancer Genomics Core, which is supported by the Cancer Prevention and Research Institute of Texas (CPRIT RP180734).

## REFERENCES

1. Green CB, Takahashi JS, and Bass J (2008). The meter of metabolism. Cell 134, 728–742. [PubMed: 18775307]
2. Guan D, and Lazar MA (2021). Interconnections between circadian clocks and metabolism. J. Clin. Invest 131, e148278. [PubMed: 34338232]
3. Eckel-Mahan K, and Sassone-Corsi P (2013). Metabolism and the circadian clock converge. Physiol. Rev 93, 107–135. [PubMed: 23303907]
4. Buijs FN, León-Mercado L, Guzmán-Ruiz M, Guerrero-Vargas NN, Romo-Nava F, and Buijs RM (2016). The Circadian System: A Regulatory Feedback Network of Periphery and Brain. Physiology 31, 170–181. [PubMed: 27053731]
5. Dibner C, Schibler U, and Albrecht U (2010). The mammalian circadian timing system: organization and coordination of central and peripheral clocks. Annu. Rev. Physiol 72, 517–549. [PubMed: 20148687]
6. Hattar S, Liao HW, Takao M, Berson DM, and Yau KW (2002). Melanopsin-containing retinal ganglion cells: architecture, projections, and intrinsic photosensitivity. Science 295, 1065–1070. [PubMed: 11834834]
7. Stokkan KA, Yamazaki S, Tei H, Sakaki Y, and Menaker M (2001). Entrainment of the circadian clock in the liver by feeding. Science 291, 490–493. [PubMed: 11161204]
8. Damiola F, Le Minh N, Preitner N, Kornmann B, Fleury-Olela F, and Schibler U (2000). Restricted feeding uncouples circadian oscillators in peripheral tissues from the central pacemaker in the suprachiasmatic nucleus. Genes Dev 14, 2950–2961. [PubMed: 11114885]
9. Adamovich Y, Rousso-Noori L, Zwighaft Z, Neufeld-Cohen A, Golik M, Kraut-Cohen J, Wang M, Han X, and Asher G (2014). Circadian clocks and feeding time regulate the oscillations and levels of hepatic triglycerides. Cell Metab 19, 319–330. [PubMed: 24506873]
10. Hatori M, Vollmers C, Zarrinpar A, DiTacchio L, Bushong EA, Gill S, Leblanc M, Chaix A, Joens M, Fitzpatrick JAJ, et al. (2012). Time-restricted feeding without reducing caloric intake prevents metabolic diseases in mice fed a high-fat diet. Cell Metab 15, 848–860. [PubMed: 22608008]

Author Manuscript Author Manuscript Author Manuscript Author Manuscript

11. Eckel-Mahan KL, Patel VR, de Mateo S, Orozco-Solis R, Ceglia NJ, Sahar S, Dilag-Penilla SA, Dyar KA, Baldi P, and Sassone-Corsi P (2013). Reprogramming of the circadian clock by nutritional challenge. Cell 155, 1464–1478. [PubMed: 24360271]
12. Herzog ED, Hermanstyne T, Smyllie NJ, and Hastings MH (2017). Regulating the Suprachiasmatic Nucleus (SCN) Circadian Clockwork: Interplay between Cell-Autonomous and Circuit-Level Mechanisms. Cold Spring Harb. Perspect. Biol 9, a027706. [PubMed: 28049647]
13. Granados-Fuentes D, Tseng A, and Herzog ED (2006). A circadian clock in the olfactory bulb controls olfactory responsivity. J. Neurosci 26, 12219–12225. [PubMed: 17122046]
14. Eckel-Mahan KL, Phan T, Han S, Wang H, Chan GC, Scheiner ZS, and Storm DR (2008). Circadian oscillation of hippocampal MAPK activity and cAMP: implications for memory persistence. Nat. Neurosci 11, 1074–1082. [PubMed: 19160506]
15. Brami-Cherrier K, Lewis RG, Cervantes M, Liu Y, Tognini P, Baldi P, Sassone-Corsi P, and Borrelli E (2020). Cocaine-mediated circadian reprogramming in the striatum through dopamine D2R and PPARγ activation. Nat. Commun 11, 4448. [PubMed: 32895370]
16. McClung CA (2013). How might circadian rhythms control mood? Let me count the ways. Biol. Psychiatry 74, 242–249. [PubMed: 23558300]
17. Cedernaes J, Huang W, Ramsey KM, Waldeck N, Cheng L, Marcheva B, Omura C, Kobayashi Y, Peek CB, Levine DC, et al. (2019). Transcriptional Basis for Rhythmic Control of Hunger and Metabolism within the AgRP Neuron. Cell Metab 29, 1078–1091.e5. [PubMed: 30827863]
18. Orozco-Solis R, Aguilar-Arnal L, Murakami M, Peruquetti R, Ramadori G, Coppari R, and Sassone-Corsi P (2016). The Circadian Clock in the Ventromedial Hypothalamus Controls Cyclic Energy Expenditure. Cell Metab 23, 467–478. [PubMed: 26959185]
19. Kim ER, Xu Y, Cassidy RM, Lu Y, Yang Y, Tian J, Li DP, Van Drunen R, Ribas-Latre A, Cai ZL, et al. (2020). Paraventricular hypothalamus mediates diurnal rhythm of metabolism. Nat. Commun 11, 3794. [PubMed: 32732906]
20. Jones JR, Chaturvedi S, Granados-Fuentes D, and Herzog ED (2021). Circadian neurons in the paraventricular nucleus entrain and sustain daily rhythms in glucocorticoids. Nat. Commun 12, 5763. [PubMed: 34599158]
21. Adlanmerini M, Nguyen HC, Krusen BM, Teng CW, Geisler CE, Peed LC, Carpenter BJ, Hayes MR, and Lazar MA (2021). Hypothalamic REV-ERB nuclear receptors control diurnal food intake and leptin sensitivity in diet-induced obese mice. J. Clin. Invest 131, e140424. [PubMed: 33021965]
22. Swaab DF, Purba JS, and Hofman MA (1995). Alterations in the hypothalamic paraventricular nucleus and its oxytocin neurons (putative satiety cells) in Prader-Willi syndrome: a study of five cases. J. Clin. Endocrinol. Metab 80, 573–579. [PubMed: 7852523]
23. Michaud JL, Boucher F, Melnyk A, Gauthier F, Goshu E, Lévy E, Mitchell GA, Himms-Hagen J, and Fan CM (2001). Sim1 haploinsufficiency causes hyperphagia, obesity and reduction of the paraventricular nucleus of the hypothalamus. Hum. Mol. Genet 10, 1465–1473. [PubMed: 11448938]
24. Shah BP, Vong L, Olson DP, Koda S, Krashes MJ, Ye C, Yang Z, Fuller PM, Elmquist JK, and Lowell BB (2014). MC4R-expressing glutamatergic neurons in the paraventricular hypothalamus regulate feeding and are synaptically connected to the parabrachial nucleus. Proc. Natl. Acad. Sci. USA 111, 13193–13198. [PubMed: 25157144]
25. An JJ, Liao GY, Kinney CE, Sahibzada N, and Xu B (2015). Discrete BDNF Neurons in the Paraventricular Hypothalamus Control Feeding and Energy Expenditure. Cell Metab 22, 175–188. [PubMed: 26073495]
26. Li MM, Madara JC, Steger JS, Krashes MJ, Balthasar N, Campbell JN, Resch JM, Conley NJ, Garfield AS, and Lowell BB (2019). The Paraventricular Hypothalamus Regulates Satiety and Prevents Obesity via Two Genetically Distinct Circuits. Neuron 102, 653–667.e6. [PubMed: 30879785]
27. Abe M, Herzog ED, Yamazaki S, Straume M, Tei H, Sakaki Y, Menaker M, and Block GD (2002). Circadian rhythms in isolated brain regions. J. Neurosci 22, 350–356. [PubMed: 11756518]

Author Manuscript Author Manuscript Author Manuscript Author Manuscript

28. Kondratov RV, Kondratova AA, Gorbacheva VY, Vykhovanets OV, and Antoch MP (2006). Early aging and age-related pathologies in mice deficient in BMAL1, the core componentof the circadian clock. Genes Dev 20, 1868–1873. [PubMed: 16847346]

29. Paschos GK, Ibrahim S, Song WL, Kunieda T, Grant G, Reyes TM, Bradfield CA, Vaughan CH, Eiden M, Masoodi M, et al. (2012). Obesity in mice with adipocyte-specific deletion of clock component Arntl. Nat. Med 18, 1768–1777. [PubMed: 23142819]

30. Lamia KA, Storch KF, and Weitz CJ (2008). Physiological significance of a peripheral tissue circadian clock. Proc. Natl. Acad. Sci. USA 105, 15172–15177. [PubMed: 18779586]

31. Marcheva B, Ramsey KM, Buhr ED, Kobayashi Y, Su H, Ko CH, Ivanova G, Omura C, Mo S, Vitaterna MH, et al. (2010). Disruption of the clock components CLOCK and BMAL1 leads to hypoinsulinaemia and diabetes. Nature 466, 627–631. [PubMed: 20562852]

32. Izumo M, Pejchal M, Schook AC, Lange RP, Walisser JA, Sato TR, Wang X, Bradfield CA, and Takahashi JS (2014). Differential effects of light and feeding on circadian organization of peripheral clocks in a forebrain Bmal1 mutant. Elife 3, e04617. [PubMed: 25525750]

33. Mieda M, and Sakurai T (2011). Bmal1 in the nervous system is essential for normal adaptation of circadian locomotor activity and food intake to periodic feeding. J. Neurosci 31, 15391–15396. [PubMed: 22031885]

34. Husse J, Zhou X, Shostak A, Oster H, and Eichele G (2011). Synaptotagmin10-Cre, a driver to disrupt clock genes in the SCN. J. Biol. Rhythms 26, 379–389. [PubMed: 21921292]

35. Barca-Mayo O, Pons-Espinal M, Follert P, Armirotti A, Berdondini L, and De Pietri Tonelli D (2017). Astrocyte deletion of Bmal1 alters daily locomotor activity and cognitive functions via GABA signalling. Nat. Commun 8, 14336. [PubMed: 28186121]

36. Barca-Mayo O, Boender AJ, Armirotti A, and De Pietri Tonelli D (2020). Deletion of astrocytic BMAL1 results in metabolic imbalance and shorter lifespan in mice. Glia 68, 1131–1147. [PubMed: 31833591]

37. Lananna BV, Nadarajah CJ, Izumo M, Cedeño MR, Xiong DD, Dimitry J, Tso CF, McKee CA, Griffin P, Sheehan PW, et al. (2018). Cell-Autonomous Regulation of Astrocyte Activation by the Circadian Clock Protein BMAL1. Cell Rep 25, 1–9.e5. [PubMed: 30282019]

38. Patton AP, Smyllie NJ, Chesham JE, and Hastings MH (2022). Astrocytes sustain circadian oscillation and bidirectionally determine circadian period, but do not regulate circadian phase in the suprachiasmatic nucleus. J. Neurosci 42, 5522–5537. [PubMed: 35610047]

39. Koike N, Yoo SH, Huang HC, Kumar V, Lee C, Kim TK, and Takahashi JS (2012). Transcriptional architecture and chromatin landscape of the core circadian clock in mammals. Science 338, 349–354. [PubMed: 22936566]

40. Rey G, Cesbron F, Rougemont J, Reinke H, Brunner M, and Naef F (2011). Genome-wide and phase-specific DNA-binding rhythms of BMAL1 control circadian output functions in mouse liver. PLoS Biol 9, e1000595. [PubMed: 21364973]

41. Menet JS, Pescatore S, and Rosbash M (2014). CLOCK:BMAL1 is a pioneer-like transcription factor. Genes Dev 28, 8–13. [PubMed: 24395244]

42. Beytebiere JR, Trott AJ, Greenwell BJ, Osborne CA, Vitet H, Spence J, Yoo SH, Chen Z, Takahashi JS, Ghaffari N, and Menet JS (2019). Tissue-specific BMAL1 cistromes reveal that rhythmic transcription is associated with rhythmic enhancer-enhancer interactions. Genes Dev 33, 294–309. [PubMed: 30804225]

43. Hatanaka F, Matsubara C, Myung J, Yoritaka T, Kamimura N, Tsutsumi S, Kanai A, Suzuki Y, Sassone-Corsi P, Aburatani H, et al. (2010). Genome-wide profiling of the core clock protein BMAL1 targets reveals a strict relationship with metabolism. Mol. Cell Biol 30, 5636–5648. [PubMed: 20937769]

44. Cervantes M, Forné I, Ranjit S, Gratton E, Imhof A, and Sassone-Corsi P (2020). BMAL1 Associates with NOP58 in the Nucleolus and Contributes to Pre-rRNA Processing. iScience 23, 101151. [PubMed: 32450515]

45. Wen S, Ma D, Zhao M, Xie L, Wu Q, Gou L, Zhu C, Fan Y, Wang H, and Yan J (2020). Spatiotemporal single-cell analysis of gene expression in the mouse suprachiasmatic nucleus. Nat. Neurosci 23, 456–467. [PubMed: 32066983]

Author Manuscript
Author Manuscript
Author Manuscript
Author Manuscript

46. Steuernagel L, Lam BYH, Klemm P, Dowsett GKC, Bauder CA, Tadross JA, Hitschfeld TS, Del Rio Martin A, Chen W, de Solis AJ, et al. (2022). HypoMap-a unified single-cell gene expression atlas of the murine hypothalamus. Nat. Metab 4, 1402–1419. [PubMed: 36266547]

47. Mickelsen LE, Bolisetty M, Chimileski BR, Fujita A, Beltrami EJ, Costanzo JT, Naparstek JR, Robson P, and Jackson AC (2019). Single-cell transcriptomic analysis of the lateral hypothalamic area reveals molecularly distinct populations of inhibitory and excitatory neurons. Nat. Neurosci 22, 642–656. [PubMed: 30858605]

48. Lopez JP, Brivio E, Santambrogio A, De Donno C, Kos A, Peters M, Rost N, Czamara D, Brückl TM, Roeh S, et al. (2021). Single-cell molecular profiling of all three components of the HPA axis reveals adrenal ABCB1 as a regulator of stress adaptation. Sci. Adv 7, eabe4497. [PubMed: 33571131]

49. Stuart T, Butler A, Hoffman P, Hafemeister C, Papalexi E, Mauck WM 3rd, Hao Y, Stoeckius M, Smibert P, and Satija R (2019). Comprehensive Integration of Single-Cell Data. Cell 177, 1888–1902.e21. [PubMed: 31178118]

50. Xu Y, Wu Z, Sun H, Zhu Y, Kim ER, Lowell BB, Arenkiel BR, Xu Y, and Tong Q (2013). Glutamate mediates the function of melanocortin receptor 4 on Sim1 neurons in body weight regulation. Cell Metab 18, 860–870. [PubMed: 24315371]

51. Wu Z, Xu Y, Zhu Y, Sutton AK, Zhao R, Lowell BB, Olson DP, and Tong Q (2012). An obligate role of oxytocin neurons in diet induced energy expenditure. PLoS One 7, e45167. [PubMed: 23028821]

52. Brancaccio M, Edwards MD, Patton AP, Smyllie NJ, Chesham JE, Maywood ES, and Hastings MH (2019). Cell-autonomous clock of astrocytes drives circadian behavior in mammals. Science 363, 187–192. [PubMed: 30630934]

53. Wahis J, Baudon A, Althammer F, Kerspern D, Goyon S, Hagiwara D, Lefevre A, Barteczko L, Boury-Jamot B, Bellanger B, et al. (2021). Astrocytes mediate the effect of oxytocin in the central amygdala on neuronal activity and affective states in rodents. Nat. Neurosci 24, 529–541. [PubMed: 33589833]

54. Althammer F, Wimmer MC, Krabichler Q, Küppers S, Schimmer J, Fröhlich H, Dötsch L, Gruber T, Wunsch S, Schubert T, et al. (2022). Analysis of the hypothalamic oxytocin system and oxytocin receptor-expressing astrocytes in a mouse model of Prader-Willi syndrome. J. Neuroendocrinol 34, e13217. [PubMed: 36458331]

55. Kim JD, Yoon NA, Jin S, and Diano S (2019). Microglial UCP2 Mediates Inflammation and Obesity Induced by High-Fat Feeding. Cell Metab 30, 952–962.e5. [PubMed: 31495690]

56. Gao Y, Tschöp MH, and Luquet S (2014). Hypothalamic tanycytes: gatekeepers to metabolic control. Cell Metab 19, 173–175. [PubMed: 24506860]

57. Gao S, Dai Y, and Rehman J (2021). A Bayesian inference transcription factor activity model for the analysis of single-cell transcriptomes. Genome Res 31, 1296–1311. [PubMed: 34193535]

58. Qu M, Duffy T, Hirota T, and Kay SA (2018). Nuclear receptor HNF4A transrepresses CLOCK:BMAL1 and modulates tissue-specific circadian networks. Proc. Natl. Acad. Sci. USA 115, E12305–E12312. [PubMed: 30530698]

59. Morton GJ, Thatcher BS, Reidelberger RD, Ogimoto K, Wolden-Hanson T, Baskin DG, Schwartz MW, and Blevins JE (2012). Peripheral oxytocin suppresses food intake and causes weight loss in diet-induced obese rats. Am. J. Physiol. Endocrinol. Metab 302, E134–E144. [PubMed: 22008455]

60. Cheung VG, Nowak N, Jang W, Kirsch IR, Zhao S, Chen XN, Furey TS, Kim UJ, Kuo WL, Olivier M, et al. (2001). Integration of cytogenetic landmarks into the draft sequence of the human genome. Nature 409, 953–958. [PubMed: 11237021]

61. Li E, Wang L, Wang D, Chi J, Lin Z, Smith GI, Klein S, Cohen P, and Rosen ED (2024). Control of lipolysis by a population of oxytocinergic sympathetic neurons. Nature 625, 175–180. [PubMed: 38093006]

62. Vitaterna MH, King DP, Chang AM, Kornhauser JM, Lowrey PL, McDonald JD, Dove WF, Pinto LH, Turek FW, and Takahashi JS (1994). Mutagenesis and mapping of a mouse gene, Clock, essential for circadian behavior. Science 264, 719–725. [PubMed: 8171325]

Author Manuscript Author Manuscript Author Manuscript Author Manuscript

63. Bunger MK, Wilsbacher LD, Moran SM, Clendenin C, Radcliffe LA, Hogenesch JB, Simon MC, Takahashi JS, and Bradfield CA (2000). Mop3 is an essential component of the master circadian pacemaker in mammals. Cell 103, 1009–1017. [PubMed: 11163178]
64. van der Horst GT, Muijtjens M, Kobayashi K, Takano R, Kanno S, Takao M, de Wit J, Verkerk A, Eker AP, van Leenen D, et al. (1999). Mammalian Cry1 and Cry2 are essential for maintenance of circadian rhythms. Nature 398, 627–630. [PubMed: 10217146]
65. Zheng B, Larkin DW, Albrecht U, Sun ZS, Sage M, Eichele G, Lee CC, and Bradley A (1999). The mPer2 gene encodes a functional component of the mammalian circadian clock. Nature 400, 169–173. [PubMed: 10408444]
66. Earnest DJ, and Olschowka JA (1993). Circadian regulation of c-fos expression in the suprachiasmatic pacemaker by light. J. Biol. Rhythms 8, S65–S71. [PubMed: 8274764]
67. Stratmann M, Suter DM, Molina N, Naef F, and Schibler U (2012). Circadian Dbp Transcription Relies on Highly Dynamic BMAL1-CLOCK Interaction with E Boxes and Requires the Proteasome. Mol. Cell 48, 277–287. [PubMed: 22981862]
68. Aguilar-Arnal L, Hakim O, Patel VR, Baldi P, Hager GL, and Sassone-Corsi P (2013). Cycles in spatial and temporal chromosomal organization driven by the circadian clock. Nat. Struct. Mol. Biol 20, 1206–1213. [PubMed: 24056944]
69. Mure LS, Le HD, Benegiamo G, Chang MW, Rios L, Jillani N, Ngotho M, Kariuki T, Dkhissi-Benyahya O, Cooper HM, and Panda S (2018). Diurnal transcriptome atlas of a primate across major neural and peripheral tissues. Science 359, eaao0318. [PubMed: 29439024]
70. Trott AJ, and Menet JS (2018). Regulation of circadian clock transcriptional output by CLOCK:BMAL1. PLoS Genet 14, e1007156. [PubMed: 29300726]
71. Masri S, Rigor P, Cervantes M, Ceglia N, Sebastian C, Xiao C, Roqueta-Rivera M, Deng C, Osborne TF, Mostoslavsky R, et al. (2014). Partitioning circadian transcription by SIRT6 leads to segregated control of cellular metabolism. Cell 158, 659–672. [PubMed: 25083875]
72. Rojo D, Dal Cengio L, Badner A, Kim S, Sakai N, Greene J, Dierckx T, Mehl LC, Eisinger E, Ransom J, et al. (2023). BMAL1 loss in oligodendroglia contributes to abnormal myelination and sleep. Neuron 111, 3604–3618.e11. [PubMed: 37657440]
73. Valdearcos M, Douglass JD, Robblee MM, Dorfman MD, Stifler DR, Bennett ML, Gerritse I, Fasnacht R, Barres BA, Thaler JP, and Koliwad SK (2017). Microglial Inflammatory Signaling Orchestrates the Hypothalamic Immune Response to Dietary Excess and Mediates Obesity Susceptibility. Cell Metab 26, 185–197.e3. [PubMed: 28683286]
74. Hajdarovic KH, Yu D, Hassell LA, Evans S, Packer S, Neretti N, and Webb AE (2022). Single-cell analysis of the aging female mouse hypothalamus. Nat. Aging 2, 662–678. [PubMed: 36285248]
75. Luo D, Jin B, Zhai X, Li J, Liu C, Guo W, and Li J (2021). Oxytocin promotes hepatic regeneration in elderly mice. iScience 24, 102125. [PubMed: 33659883]
76. Dijk DJ, Duffy JF, and Czeisler CA (2000). Contribution of circadian physiology and sleep homeostasis to age-related changes in human sleep. Chronobiol. Int 17, 285–311. [PubMed: 10841208]
77. Nakamura TJ, Nakamura W, Yamazaki S, Kudo T, Cutler T, Colwell CS, and Block GD (2011). Age-related decline in circadian output. J. Neurosci 31, 10201–10205. [PubMed: 21752996]
78. Hood S, and Amir S (2017). The aging clock: circadian rhythms and later life. J. Clin. Invest 127, 437–446. [PubMed: 28145903]
79. Nakata M, Kumari P, Kita R, Katsui N, Takeuchi Y, Kawaguchi T, Yamazaki T, Zhang B, Shimba S, and Yada T (2021). Circadian Clock Component BMAL1 in the Paraventricular Nucleus Regulates Glucose Metabolism. Nutrients 13, 4487. [PubMed: 34960038]
80. Santoso P, Nakata M, Ueta Y, and Yada T (2018). Suprachiasmatic vasopressin to paraventricular oxytocin neurocircuit in the hypothalamus relays light reception to inhibit feeding behavior. Am. J. Physiol. Endocrinol. Metab 315, E478–E488. [PubMed: 28174180]
81. Zhang G, and Cai D (2011). Circadian intervention of obesity development via resting-stage feeding manipulation or oxytocin treatment. Am. J. Physiol. Endocrinol. Metab 301, E1004–E1012. [PubMed: 21828335]

Author Manuscript Author Manuscript Author Manuscript Author Manuscript

82. Wolff CA, Gutierrez-Monreal MA, Meng L, Zhang X, Douma LG, Costello HM, Douglas CM, Ebrahimi E, Pham A, Oliveira AC, et al. (2023). Defining the age-dependent and tissue-specific circadian transcriptome in male mice. Cell Rep 42, 111982. [PubMed: 36640301]

83. Li H, and Durbin R (2009). Fast and accurate short read alignment with Burrows-Wheeler transform. Bioinformatics 25, 1754–1760. [PubMed: 19451168]

84. Li H, Handsaker B, Wysoker A, Fennell T, Ruan J, Homer N, Marth G, Abecasis G, and Durbin R; 1000 Genome Project Data Processing Subgroup (2009). The Sequence Alignment/Map format and SAMtools. Bioinformatics 25, 2078–2079. [PubMed: 19505943]

85. Zhang Y, Liu T, Meyer CA, Eeckhoute J, Johnson DS, Bernstein BE, Nusbaum C, Myers RM, Brown M, Li W, and Liu XS (2008). Model-based analysis of ChIP-Seq (MACS). Genome Biol 9, R137. [PubMed: 18798982]

86. Dobin A, Davis CA, Schlesinger F, Drenkow J, Zaleski C, Jha S, Batut P, Chaisson M, and Gingeras TR (2013). STAR: ultrafast universal RNA-seq aligner. Bioinformatics 29, 15–21. [PubMed: 23104886]

87. Quinlan AR, and Hall IM (2010). BEDTools: a flexible suite of utilities for comparing genomic features. Bioinformatics 26, 841–842. [PubMed: 20110278]

88. Robinson JT, Thorvaldsdóttir H, Winckler W, Guttman M, Lander ES, Getz G, and Mesirov JP (2011). Integrative genomics viewer. Nat. Biotechnol 29, 24–26. [PubMed: 21221095]

89. Yu G, Wang LG, and He QY (2015). ChIPseeker: an R/Bioconductor package for ChIP peak annotation, comparison and visualization. Bioinformatics 31, 2382–2383. [PubMed: 25765347]

90. Heinz S, Benner C, Spann N, Bertolino E, Lin YC, Laslo P, Cheng JX, Murre C, Singh H, and Glass CK (2010). Simple combinations of lineage-determining transcription factors prime cis-regulatory elements required for macrophage and B cell identities. Mol. Cell 38, 576–589. [PubMed: 20513432]

91. Butler A, Hoffman P, Smibert P, Papalexi E, and Satija R (2018). Integrating single-cell transcriptomic data across different conditions, technologies, and species. Nat. Biotechnol 36, 411–420. [PubMed: 29608179]

92. Becht E, McInnes L, Healy J, Dutertre CA, Kwok IWH, Ng LG, Ginhoux F, and Newell EW (2018). Dimensionality reduction for visualizing single-cell data using UMAP. Nat. Biotechnol 10.1038/nbt.4314.

93. McGinnis CS, Murrow LM, and Gartner ZJ (2019). DoubletFinder: Doublet Detection in Single-Cell RNA Sequencing Data Using Artificial Nearest Neighbors. Cell Syst 8, 329–337.e4. [PubMed: 30954475]

94. Hughes ME, Hogenesch JB, and Kornacker K (2010). JTK_CYCLE: an efficient nonparametric algorithm for detecting rhythmic components in genome-scale data sets. J. Biol. Rhythms 25, 372–380. [PubMed: 20876817]

95. Parsons R, Parsons R, Garner N, Oster H, and Rawashdeh O (2020). CircaCompare: a method to estimate and statistically support differences in mesor, amplitude and phase, between circadian rhythms. Bioinformatics 36, 1208–1212. [PubMed: 31588519]

96. Ge SX, Jung D, and Yao R (2020). ShinyGO: a graphical gene-set enrichment tool for animals and plants. Bioinformatics 36, 2628–2629. [PubMed: 31882993]

97. Xu P, Berto S, Kulkarni A, Jeong B, Joseph C, Cox KH, Greenberg ME, Kim TK, Konopka G, and Takahashi JS (2021). NPAS4 regulates the transcriptional response of the suprachiasmatic nucleus to light and circadian behavior. Neuron 109, 3268–3282.e6. [PubMed: 34416169]

Author Manuscript Author Manuscript Author Manuscript Author Manuscript

## Highlights

- Loss of BMAL1 in the PVN leads to arrhythmic energy intake and energy expenditure
- TRF improves rhythmicity in BMAL1-PVN KO mice
- BMAL1 binds PVN target genes, driving highly diurnal and cell-specific gene expression
- Diurnal OXT secretion is driven by PVN BMAL1 and important for rhythmicity in behavior

Author Manuscript

Author Manuscript

Author Manuscript

Author Manuscript

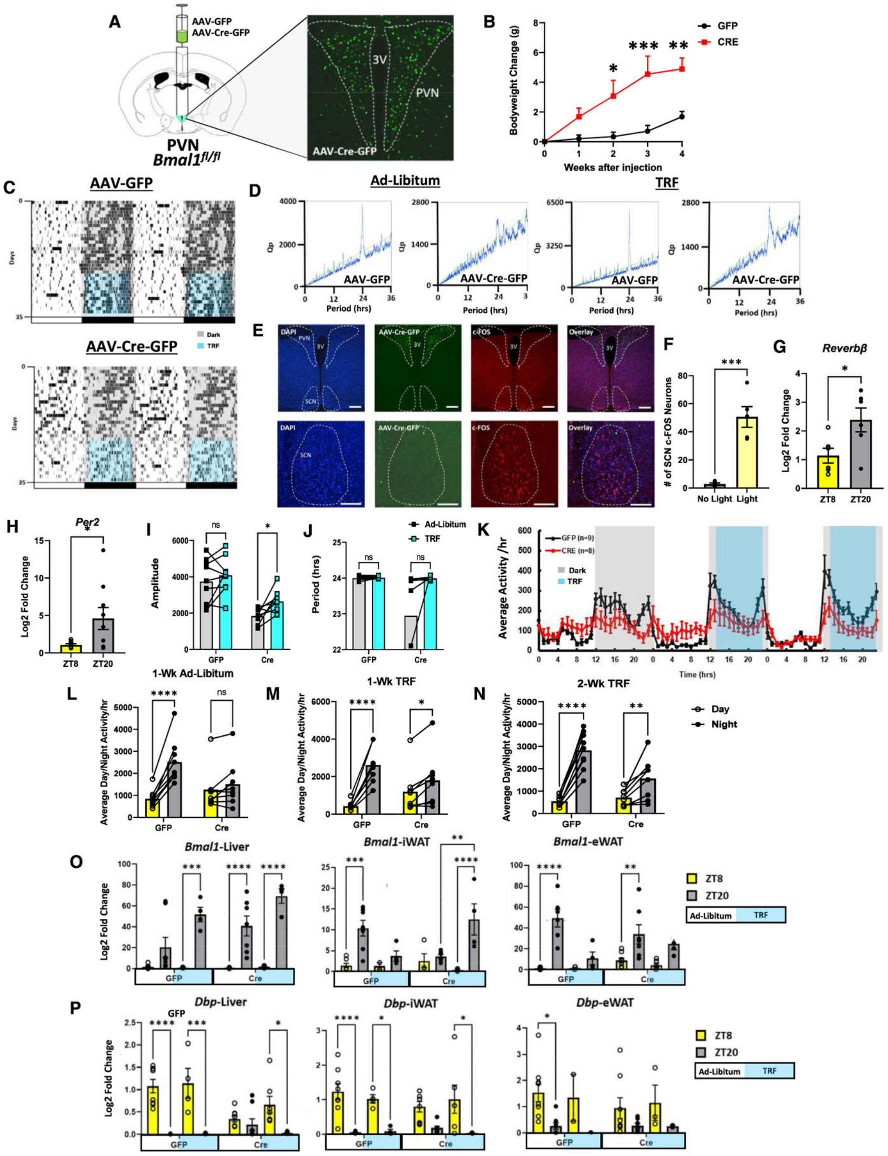

**Figure 1. PVN BMAL1 regulates diurnal activity and energy balance**

(A) Experimental schematic. *Bmal1*$^{fl/fl}$ mice were injected with AAVDJ8-CMV-GFP (WT control) or AAV5-CMV-Cre-GFP (BMAL1-PVN KO) bilaterally into the PVN.

(B) Bodyweight of virus-injected *Bmal1*$^{fl/fl}$ mice (two-way ANOVA with Sidak's multiple comparisons, $N = 10$, $F(4,72) = 7.452$, $*p < 0.05$, $**p < 0.01$, $***p < 0.001$).

(C) Daily home cage locomotion of AAVDJ8-CMV-GFP-injected (top) and AAV5-CMV-Cre-GFP-injected (bottom) mice, measured via infrared sensors, and double-plotted actograms of activity during *ad libitum* and time-restricted feeding (TRF) (light blue shading).

(D) Periodograms for mice in (C).

(E) Immunofluorescence of SCN c-Fos following a 30-min light pulse at circadian time 19 (CT19).

Author Manuscript Author Manuscript Author Manuscript Author Manuscript

(F) Quantification of c-Fos-positive SCN neurons in mice exposed to or devoid of light (scale bar, 100 μM; unpaired t test, $N = 4$ biological replicates, $t = 5.716$, df = 7, $^{***}p < 0.001$).

(G and H) Amplitude (G) and period (H) of mouse activity under *ad libitum* and TRF (two-way ANOVA, Sidak's multiple comparisons, for GFP $N = 9$, for Cre $N = 8$, $F(1,15) = 1.187$, $^{*}p < 0.05$).

(I) Weekly average activity per hour across 24 h under *ad libitum* or TRF.

(J–L) Average total daily activity in virus-injected mice during *ad libitum* feeding (J) or week 1 (K) and 2 (L) of TRF (two-way ANOVA with Sidak's multiple comparisons, for GFP $N = 9$, for Cre $N = 8$, $F(1,15) = 27.34$, $^{**}p < 0.01$, $^{****}p < 0.0001$).

(M and N) qPCR showing mRNA expression of *Bmal1* (N) and *Dbp* (N) in liver and adipose tissue of *Bmal1*-PVN KO and control mice under *ad libitum* or TRF (two-way ANOVA with Sidak's multiple comparisons, $N = 3–5$ biological replicates).

Author Manuscript

Author Manuscript

Author Manuscript

Author Manuscript

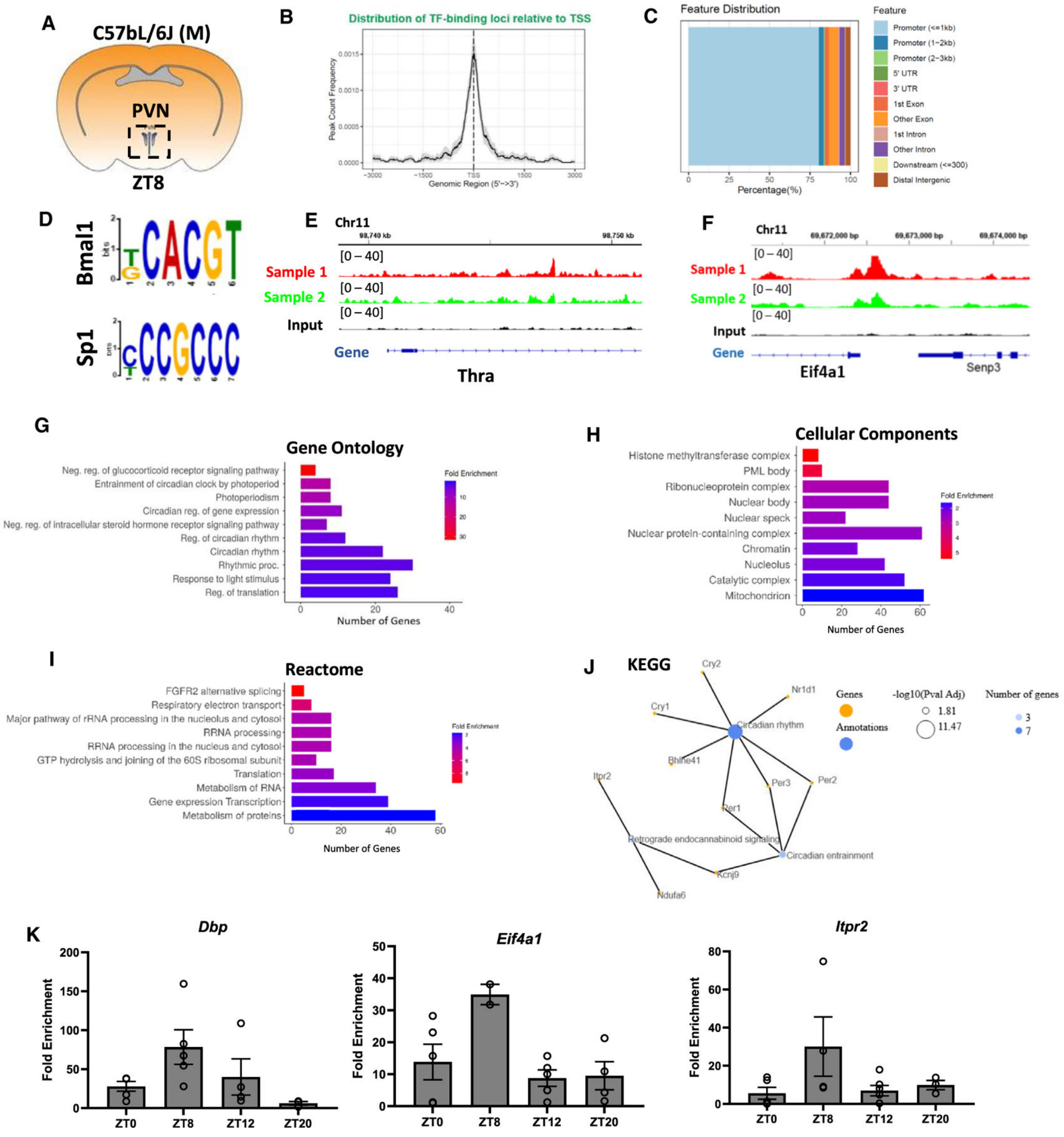

**Figure 2. ChIP-seq reveals widespread genomic regulation by BMAL1 in the PVN**

(A) Experimental scheme: C57BL/6J mice 10–12 weeks old were sacrificed at zeitgeber time 8 (ZT8) for PVN-enriched tissue (pooled), followed by BMAL1 ChIP-seq ($N = 2$ biological replicates).

(B and C) Distribution of BMAL1 binding sites relative to the transcriptional start site (TSS) (B) and the feature distribution (C) of binding.

(D) Motif analysis reveals the top motifs represented in BMAL1 targets.

(E–I) Integrated Genome Viewer peak visualization of *Thra* and *Eif4a* and (G–I) functional enrichment of the top 10 Gene Ontology (G), molecular functions (H), and reactome (I) pathways (false discovery rate cutoff: 0.05) of PVN BMAL1 target sites.

(J) KEGG network of ChIP-seq-identified genes.

(K) ChIP-qPCR from enriched PVN tissue harvested at different ZTs shows BMAL1 binding at target sites for *Dbp*, *Eif4a1*, and *Itpr2*; $N = 2$–5 biological replicates.

Author Manuscript

Author Manuscript

Author Manuscript

Author Manuscript

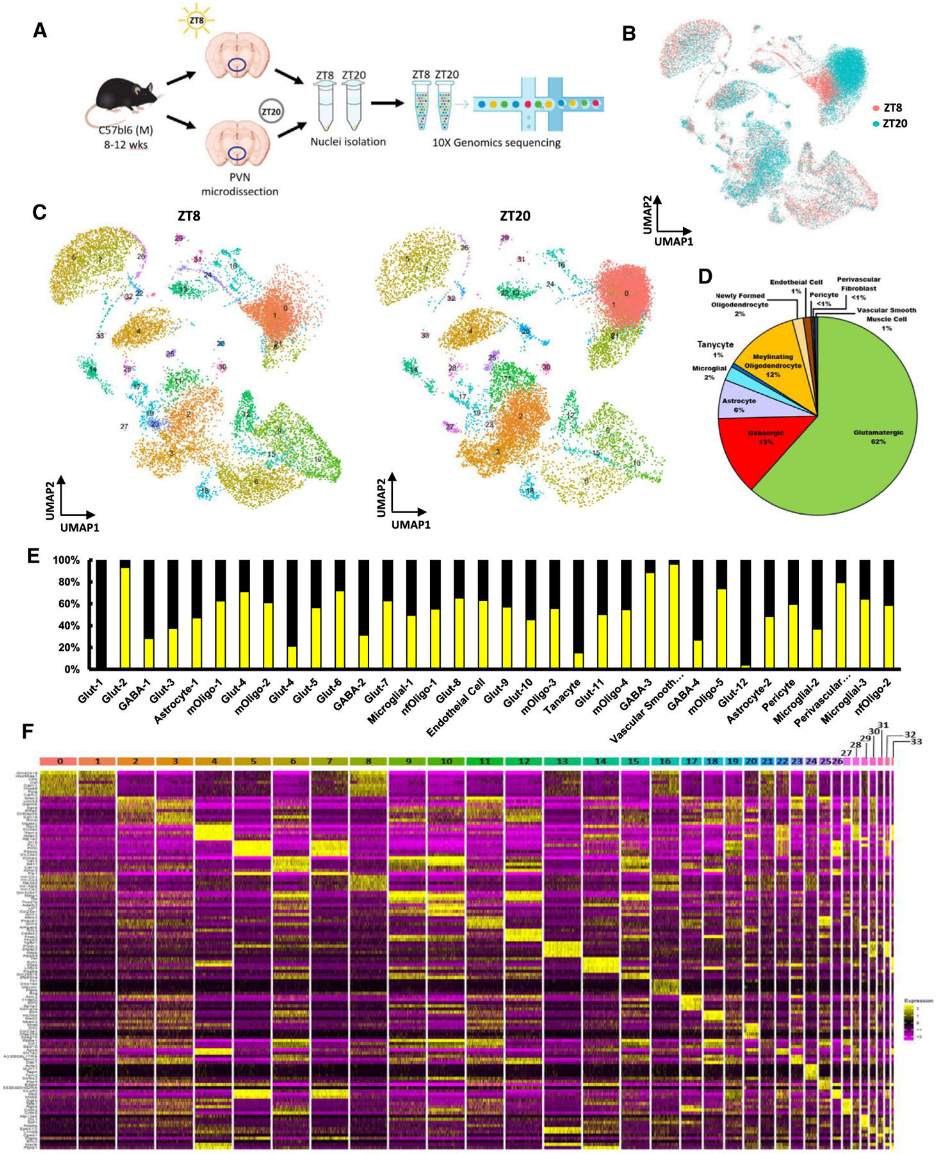

**Figure 3. snRNA-seq shows cell-specific diurnally variant gene expression in the PVN**

(A) Single-nucleus RNA sequencing (snRNA-seq) schematic of nucleus isolation from the PVNs of mice dissected at ZT8 (daytime) or ZT20 (nighttime).

(B) Uniform manifold approximation and projection (UMAP) plot of integrated nuclei colored by their ZT collection time (cluster resolution 0.8).

(C) UMAP of nuclei colored and labeled according to each cell cluster.

(D) Percentage of identified cell types.

(E) Nucleus distribution for each cluster. Bars correspond to nuclei from sampled libraries prepared from PVNs collected in the light (ZT8, yellow) or dark (ZT20, black).

(F) Integrated heatmap of combined ZT PVN snRNA-seq data, with the top eight genes (left) distinguishing each of the 34 clusters (top).

Author Manuscript Author Manuscript Author Manuscript Author Manuscript

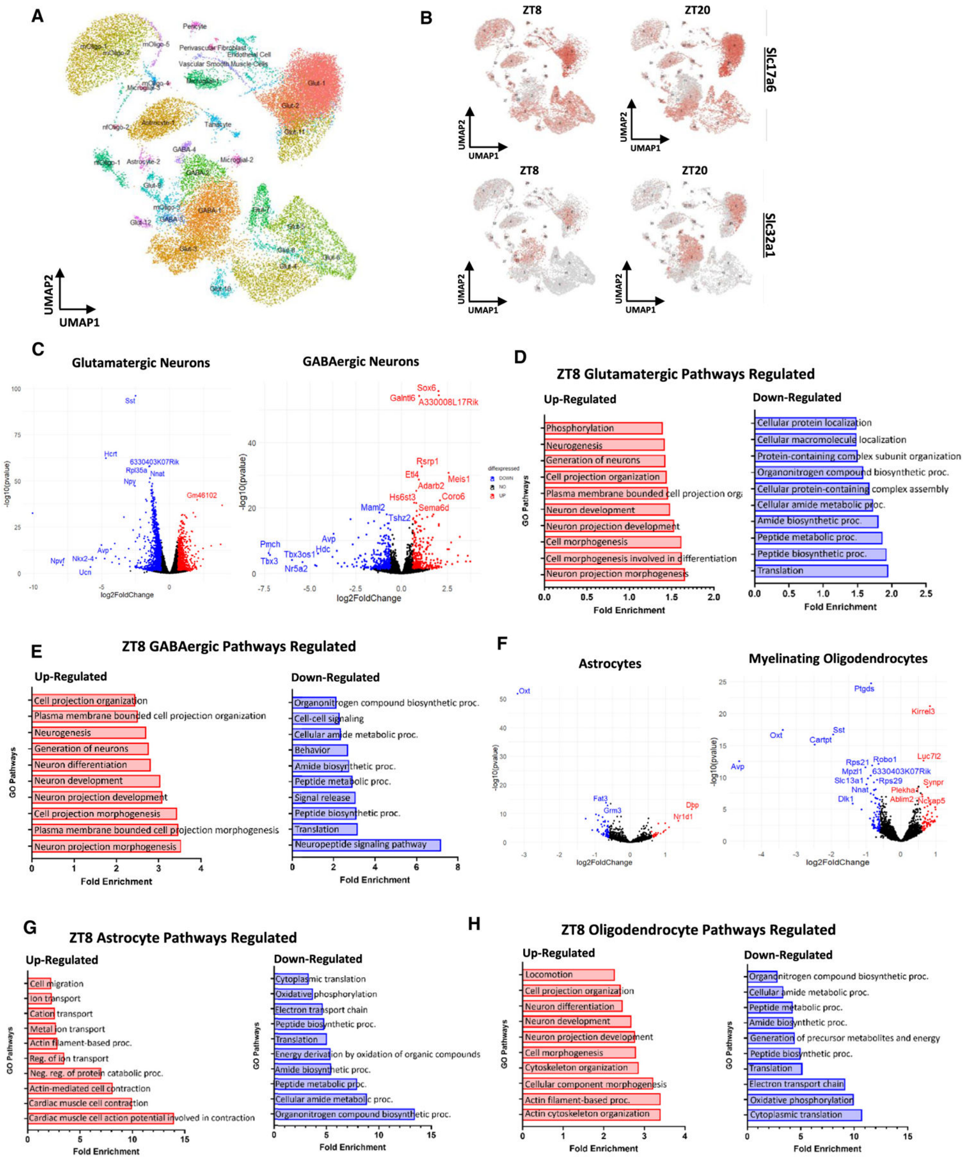

**Figure 4. Diurnally divergent gene expression in GABAergic and glutamatergic neuronal cluster subtypes within the PVN**

(A) UMAP of PVN snRNA-seq with neuronal clusters outlined.

(B) UMAPs highlight the diurnal expression of the cluster-identifying cell markers *Slc17a6* (top, glutamatergic) and *Slc32a1* (bottom, GABAergic).

(C) Volcano plots of DEGs for pseudobulked clusters ($\log_2$FC ≥ 0.3, $p < 0.05$). Blue and red points represent significantly down- and up-regulated genes ZT8 compared to ZT20.

(D and E) Top Gene Ontology pathways corresponding to upregulated (red) and downregulated (blue) genes at ZT8 in glutamatergic (D) and GABAergic (E) pseudobulked clusters.

(F–H) Volcano plots showing diurnally expressed DEGs from pseudobulked astrocytes (right) and myelinating oligodendrocytes (left) ($\log_2$FC ≥ 0.3, $p < 0.05$). Top Gene Ontology pathways corresponding to upregulated (red) and downregulated (blue) genes at ZT8 in astrocyte (G) and myelinating oligodendrocyte (H) pseudobulked clusters.

Author Manuscript Author Manuscript Author Manuscript Author Manuscript

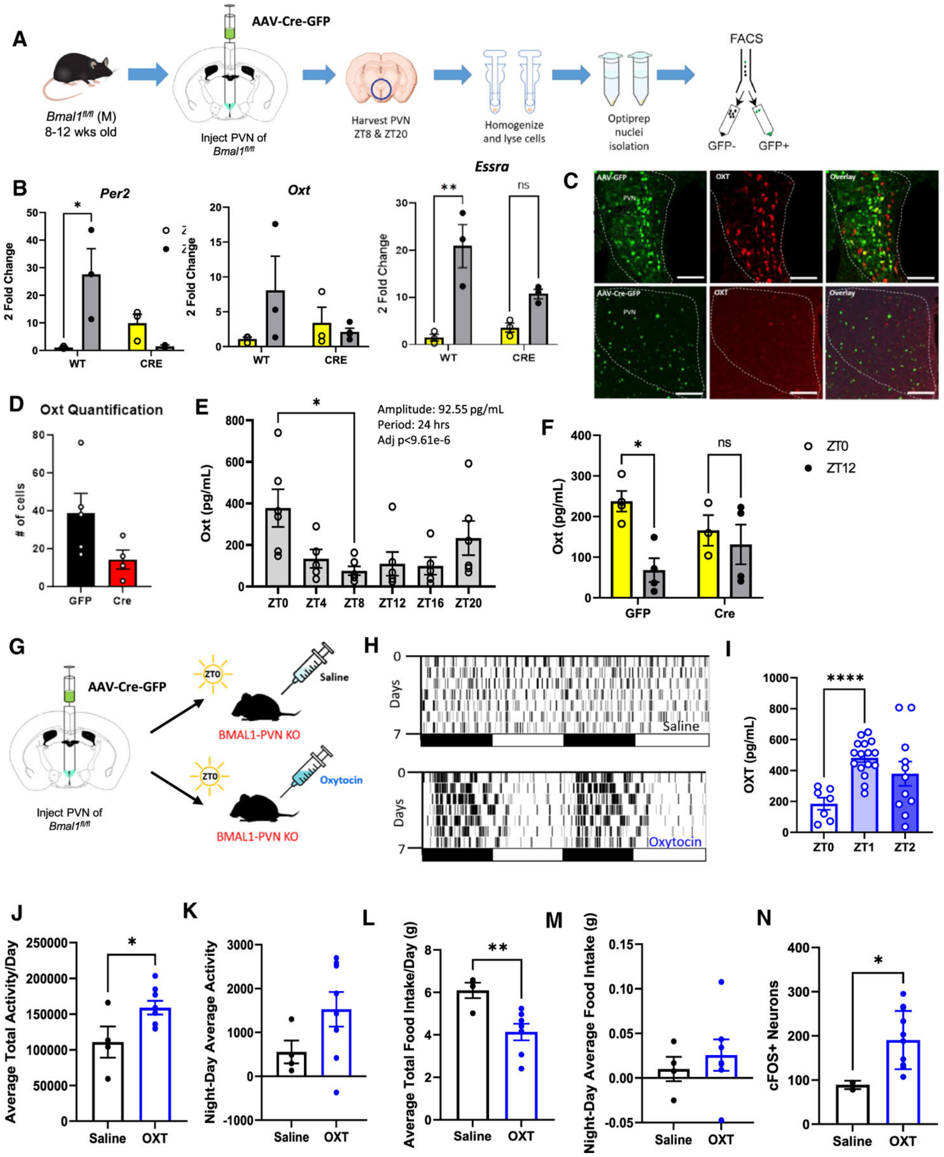

**Figure 5. OXT expression in the PVN is regulated by BMAL1**

(A) Experimental workflow of nuclei isolation and sorting of GFP-positive nuclei from BMAL1-PVN KO mice.

(B) Gene expression of *Per2*, *Oxt*, and *Essra* in WT PVN and GFP-positive BMAL1 KO nuclei sorted by fluorescence-activated cell sorting (mixed-effects analysis, $N = 2–3$ technical replicates, $*p = .0171$).

(C and D) OXT expression and quantification in WT (AAV-GFP) and BMAL1-PVN KO (AAV-Cre-GFP) mouse PVNs at ZT8 (C) (scale bar, 100 μM) and Localization of OXT at ZT8 vs. ZT20, highlighted by white arrows (D) (scale bar, 100 μM).

(E) *Oxt* levels across 4 h in control mice measured via ELISA (one way ANOVA with Tukey's multiple comparisons, $N = 6$, $F(5,23) = 2.962$, $*p < 0.05$) and JTK analysis.

(F) Serum OXT at ZT0 and ZT12 in WT and PVN BMAL-KO mice.

(G) Schematic of OXT or vehicle injections.

Author Manuscript

Author Manuscript

Author Manuscript

Author Manuscript

(H) Actograms reveal the individual activity rhythms of control- and OXT-injected mice.

(I) Serum OXT of mice before and 1 h and 2 h (ZT1 and ZT2, respectively) after OXT injection (one-way ANOVA, ZT0 $N = 7$, ZT1 $N = 16$, and ZT2 $N = 11$; $t = 5.96$, $df = 21$, $^{****}p < 0.0001$).

(J) Average total activity per day (unpaired t test, saline $N = 4$ and OXT $N = 8$, $t = 2.37$, $df = 10$, $^{*}p < 0.05$).

(K) Night vs. day activity in each injection group.

(L) Average food intake in control and OXT-injected mice over 3 days and total and average day/night food consumption (unpaired t test, saline $N = 4$ and OXT $N = 7$, $t = 3.32$, $df = 9$, $^{**}p < 0.01$).

(M) Difference between night and day average food intake.

(N) Quantification of PVN cFOS-positive cells in control vs. OXT-injected mice (unpaired t test, saline $N = 3$ and OXT $N = 11$, $t = 2.58$, $df = 12$, $^{*}p < 0.05$).

Author Manuscript Author Manuscript Author Manuscript Author Manuscript

## KEY RESOURCES TABLE

| REAGENT or RESOURCE | SOURCE | IDENTIFIER |
|---|---|---|
| Antibodies | | |
| Anti-rabbit BMAL1 | Novus Biologicals | NB100-2288; RRID:AB_10000794 |
| Anti-rabbit cFOS | Cell Signaling Technology | 2250; RRID:AB_2247211 |
| DAPI | ThermoFischer | D1306; RRID:AB_2629482 |
| AlexaFlour™ 555 goat anti-rabbit | Invitrogen | A21430; RRID:AB_10374475 |
| BMAL1 (for ChIP and WB) | Abcam | ab93806; RRID:AB_10675117 |
| Normal Rabbit IgG | Cell Signaling Technology | 2729P; RRID:AB_1031062 |
| Actin | Abcam | ab119716; RRID:AB_10898702 |
| Bacterial and virus strains | | |
| AAV5-CMV-Cre-GFP | Tong Laboratory, Brown Foundation Institute for Molecular Medicine, Houston TX | (Kim et al., 2020)[19] |
| AAVDJ8-CMV-GFP | Tong Laboratory, Brown Foundation Institute for Molecular Medicine, Houston TX | (Kim et al., 2020)[19] |
| Chemicals, peptides, and recombinant proteins | | |
| Opti-Prep Density Gradient Medium | Sigma | D1556 |
| TRIzol | Thermo Fisher Scientific | 15596026 |
| Advanced Universal SYBR Green Super mix | Biorad | 1725274 |
| Artificial cerebral spinal fluid (aCSF) | R&D Systems | 3525 |
| Protector RNase inhibitor | Sigma | 3335399001 |
| Normal Saline | McKesson | 16–20069 |
| Ketamine Hydrocholoride Injection, 100 mg/mL, C3N | Dechra Vet Products | VINV-CII-0016 |
| Xylazine (100 mg/mL) | Covetrus | NDC: 11695–4024-1 |
| Carprofen | Covetrus | NDC: 11695–6935-1 |
| Oxytocin | Abcam | ab120186 |
| Aprotinin | Sigma | 10236624001 |
| Critical commercial assays | | |
| ChIP Kit | Cell Signal | 9005 |
| Amaxa™ Cell Line Nucleofector Kit V | Lonza | VCA-1003 |
| iScript cDNA Synthesis Kit | BioRad | 1708891 |
| Oxytocin ELISA Kit | Enzo Life Sciences | ADI-900–153A |
| Protease inhibitor cocktail (PIC) | Sigma | P8340 |
| EnzyChrom Free Fatty Assay Kit | BioAssay System | EFFA-100 |
| Deposited data | | |
| ChIP-seq | This paper | GEO: GSE231940 |

Author Manuscript

Author Manuscript

Author Manuscript

Author Manuscript

| **REAGENT or RESOURCE** | **SOURCE** | **IDENTIFIER** |
|---|---|---|
| snRNA-seq | This paper | GEO: GSE231734 |
| Experimental models: Cell lines | | |
| SH-SY5Y cells | Zheng Laboratory, Brown Foundation Institute for Molecular Medicine, Houston TX | NA |
| Experimental models: Organisms/strains | | |
| Mouse/B6.129S4(Cg)-Bmal1tm1Weit/J | Jackson Labs | JAX: 007668 |
| Mouse/C57bl/6J | Jackson Labs | JAX: 000664 |
| Oligonucleotides | | |
| siBmal1 | Ambion | 4390843 |
| siScramble | Ambion | 4457287 |
| Primer: Bmal1fl/fl, forward: 5′-ACTGGAAGTAACTTTATCAAACTG-3 reverse: 5′-CTGACCAACTTGCTAACAATTA-3′ | Eurofins | Kim et al., 2020[19] |
| ChIP Primer: Dbp-up<br>ACACCCGCATCCGATAGC<br>CCACTTCGGGCCAATGAG | Eurofins | NA |
| ChIP Primer: Dbp-E1<br>TCTGCAGAACTGACTGGTTGA<br>GCGTGCAAGCCTCCAGGAT | Eurofins | NA |
| ChIP Primer: Per2-TSS<br>GCGTCTCCACCAATTGATGA<br>CCCTCCGCTGTCACATAGT | Eurofins | NA |
| ChIP Primer: Per1c<br>AGCCAGGACCCAGAAAGAACTCAT<br>AACTCACTCACCCTGAACCTGCTT | Eurofins | NA |
| ChIP Primer: Itpr2<br>GGTGTGGTTGGAGGAGACAC<br>AGCCGATCAACATCTGCTTT | Eurofins | NA |
| ChIP Primer: Eif4a1<br>CCTGCTGAGCCACATGACTA<br>CGCCCTATTGGGTAGTTTGA | Eurofins | NA |
| ChIP Primer: Igsf8<br>TAGCACCCCAGTTCTTGCAG<br>GTGTGGGACTAAGAACGGCA | Eurofins | NA |
| ChIP Primer: Cpeb3<br>CATCAAGGATAAACCGGTGC<br>GAAGAATGGGGCAAACTTCC | Eurofins | NA |
| ChIP Primer: Dbp-up<br>ACACCCGCATCCGATAGC<br>CCACTTCGGGCCAATGAG | Eurofins | NA |
| ChIP Primer: Dbp-E1<br>TCTGCAGAACTGACTGGTTGA<br>GCGTGCAAGCCTCCAGGAT | Eurofins | NA |
| ChIP Primer: Per2-TSS<br>GCGTCTCCACCAATTGATGA<br>CCCTCCGCTGTCACATAGT | Eurofins | NA |
| ChIP Primer: Per1c<br>AGCCAGGACCCAGAAAGAACTCAT<br>AACTCACTCACCCTGAACCTGCTT | Eurofins | NA |

Author Manuscript

Author Manuscript

Author Manuscript

Author Manuscript

| **REAGENT or RESOURCE** | **SOURCE** | **IDENTIFIER** |
|---|---|---|
| ChIP Primer: Itpr2<br>GGTGTGGTTGGAGGAGACAC<br>AGCCGATCAACATCTGCTTT | Eurofins | NA |
| ChIP Primer: Eif4a1<br>CCTGCTGAGCCACATGACTA<br>CGCCCTATTGGGTAGTTTGA | Eurofins | NA |
| ChIP Primer: Igsf8<br>TAGCACCCCAGTTCTTGCAG<br>GTGTGGGACTAAGAACGGCA | Eurofins | NA |
| ChIP Primer: Cpeb3<br>CATCAAGGATAAACCGGTGC<br>GAAGAATGGGGCAAACTTCC | Eurofins | NA |
| ChIP Primer: Ca11<br>GCCGGCTCTGAACACCAGATC<br>GAGGAGGCGACTGAGGAATGG | Eurofins | NA |
| Human Primer: Bmal1<br>TTAGCCAACGTCCTGGAAGG<br>CCTTCTCCAGAGGGCAGCAT | Eurofins | NA |
| Human Primer: Esrralpha<br>CCGCGATGTCCTTTTGTGTCC<br>CTGTACTCGATGCTCCCCTGG | Eurofins | NA |
| Human Primer: Thra<br>TGGGCAAGTC ACTCTCTGC<br>CAAACTGCTGCTCAAGCTGC | Eurofins | NA |
| Human Primer: Eif4a1<br>CCATCCAGCAGCGAGCTATT<br>CGACCACCTCGACCGATTCT | Eurofins | NA |
| Human Primer: Adk<br>CCAAGCCCAAAAAGCTCAAGG<br>GTCATCTCGCCCTTGTGTGA | Eurofins | NA |
| Human Primer: 18s<br>AAGTCCCTGCCCTTTGTACACA<br>GATCCGAGGGCCTCACTAAAC | Eurofins | NA |
| Mouse Primer: Dbp<br>AATGACCTTTGAACCTGATCCCGCT<br>GCTCCAGTACTTCTCATCCTTCTGT | Eurofins | NA |
| Mouse Primer: Per2<br>CGCCTAGAATCCCTCCTGAGA<br>CCACCGGCCTGTAGGATCT | Eurofins | NA |
| Mouse Primer: Oxt<br>GATATGCGCAAGTGTCTCCC<br>GCGCGCTAAAGGTATTCCCA | Eurofins | NA |
| Mouse Primer: 18s<br>CGCCGCTAGAGGTGAAATTC<br>CGAACCTCCGACTTTCGTTCT | Eurofins | NA |
| Mouse Primer: Fas<br>atcccagcacttcttgatgg<br>ccgaagccaaatgagttgat | Eurofins | NA |
| Software and algorithms | | |
| R Studio 2021.9.1.372 server | R Studio | http://www.rstudio.com |
| R 4.1.1 | R | https://www.r-project.org/ |
| Prisim | GraphPad Software | https://www.graphpad.com/features |
| ClockLabs | ActiMetrics | https://www.actimetrics.com/products/clocklab/ |
| VitalView | STARR Life Sciences | https://www.starrlifesciences.com/activity/activity-software/ |

Author Manuscript Author Manuscript Author Manuscript Author Manuscript

| REAGENT or RESOURCE | SOURCE | IDENTIFIER |
|---|---|---|
| BWA | (Li and Durbin, 2009)[83] | https://github.com/lh3/bwa/releases |
| SAMtools | (Li et al., 2009)[84] | http://www.htslib.org/ |
| MACS2 | (Zhang et al., 2008)[85] | https://github.com/macs3-project/MACS |
| STAR | (Dobin et al., 2013)[86] | https://github.com/easybuilders/easybuild-easyconfigs/pull/8388 |
| bedtools | (Quinlan and Hall 2010)[87] | https://bedtools.readthedocs.io/en/latest/ |
| IGV: Integrated genome viewer | (Robinson et al., 2011)[88] | https://igv.org/ |
| Chipseeker | (Yu et al., 2015)[89] | https://www.bioconductor.org/packages/release/bioc/html/ChIPseeker.html |
| HOMER | (Heinz et al., 2010)[90] | http://homer.ucsd.edu/homer/ |
| FASTQC | Babraham Bioinformatics | https://www.bioinformatics.babraham.ac.uk/projects/fastqc/ |
| Cell Ranger | 10X Genomics | https://support.10xgenomics.com/single-cell-gene-expression/software/overview/welcome |
| R package: BITFAM | (Gao et al., 2021)[57] | https://github.com/jaleesr/BITFAM |
| R package: Seurat_4.1.0 | (Butler et al., 2018)[91] | https://satijalab.org/seurat/ |
| R package: ggplot2_3.3.6 | https://ggplot2.tidyverse.org/ | NA |
| R package: Uniform Manifold Approximation and Projection (UMAP) | (Becht et al., 2018)[92] | https://umap-learn.readthedocs.io/en/latest/ |
| R package: JTK | (Hughes et al., 2010)[94] | https://cran.r-project.org/web/packages/MetaCycle/vignettes/implementation.html |
| R package: DoubletFinder_2.0.3 | (McGinnis et al., 2019)[93] | https://github.com/chris-mcginnis-ucsf/DoubletFinder |
| R package: circaCOMPARE | (Parsons et al., 2020)[95] | https://cran.r-project.org/web/packages/circacompare/index.html |
| Python | https://www.python.org/ | NA |
| Python package jupyterlab v. 3.4.6 | https://jupyter.org/ | NA |
| Python package: pandas | https://pandas.pydata.org/ | NA |
| Python package: matplotlib | https://matplotlib.org/ | NA |
| Python package: numpy | https://doi.org/10.1038/s41586-020-2649-2 | NA |
| Python package scikit-learn | https://scikit-learn.org/ | NA |
| Other | | |
| Gene Pulser Xcell | Bio-Rad | 1652660 |
| Qsonica Q125 | Qsonica | Q125–110 |
| Bio-Rad C1000 Themocylcer | Bio-Rad | 1851196 |
| Stainless steel coronal brain matrice | Kent Scientific | RBMS-200C |
| 0.70 mm diameter micro punch | World Precision Instruments | WPKP1018 |
| 200 mg C18 Sep-Pak columns | Waters™ | WAT023620 |
| Oligonucleotides | | |
| siBmal1 | Ambion | 4390843 |
| siScramble | Ambion | 4457287 |